R93-957424-F

47 P

INVESTIGATION OF THE FEASIBILITY OF OPTICAL DIAGNOSTIC MEASUREMENTS AT THE EXIT OF THE SSME

FINAL REPORT

John A. Shirley
Laurence R. Boedeker

July 1, 1993

NASA/Marshall Space Flight Center
Contract: NAS8-36861

UNITED TECHNOLOGIES RESEARCH CENTER
East Hartford, Connecticut 06108

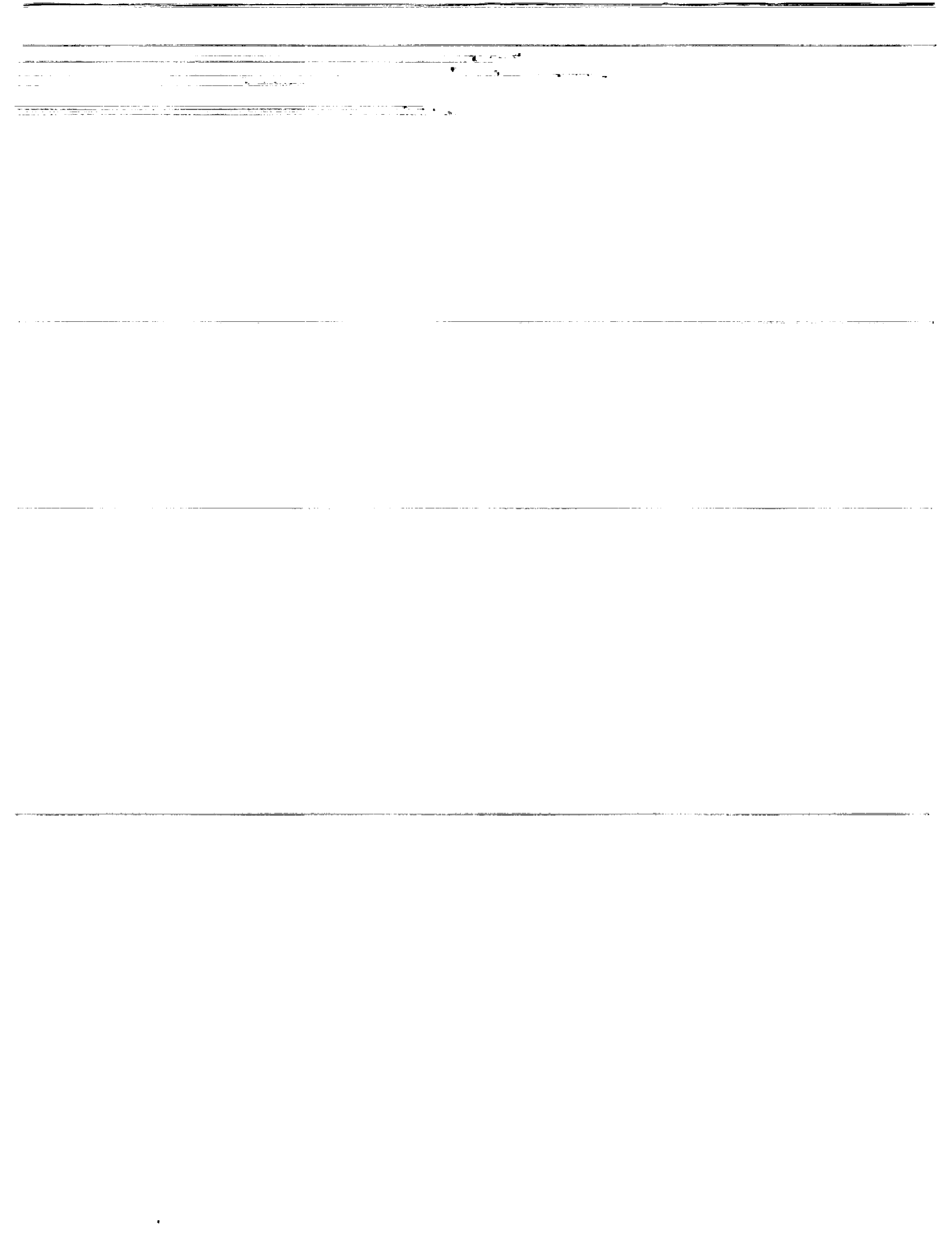

R93-957424-F

Investigation of the Feasibility of Optical Diagnostic Measurements at the Exit Plane of the SSME

INTRODUCTION

Under Contract NAS8-36861 sponsored by NASA Marshall Space Flight Center, the United Technologies Research Center is conducting an investigation of the feasibility of remote optical diagnostics to measure temperature, species concentration and velocity at the exit of the Space Shuttle Main Engine (SSME). This is a two phase study consisting of a conceptual design phase followed by a laboratory experimental investigation.

The first task of the conceptual design studies is to screen and evaluate the techniques which can be used for the measurements. The second task is to select the most promising technique or techniques, if as expected, more than one type of measurement must be used to measure all the flow variables of interest. The third task is to examine in detail analytically the capabilities and limitations of the selected technique(s). The results of this study are described in the section of this report entitled Conceptual Design Investigations.

The conceptual design studies identified spontaneous Raman scattering and photodissociative flow-tagging for measurements respectively of gas temperature and major species concentration and for velocity. These techniques and others that were considered are described in the section describing the conceptual design.

The objective of the second phase of investigations was to investigate experimentally the techniques identified in the first phase. The first task of the experimental feasibility study is to design and assemble laboratory scale experimental apparatus to evaluate the best approaches for SSME exit optical diagnostics for temperature, species concentrations and velocity, as selected in the Phase I conceptual design study. The second task is to evaluate performance, investigate limitations, and establish actual diagnostic capabilities, accuracies and precision for the selected optical systems. The third task is to evaluate design requirements and system trade-offs of conceptual instruments.

Spontaneous Raman scattering excited by a KrF excimer laser pulse was investigated for SSME exit plane temperature and major species concentration measurements. The relative concentrations of molecular hydrogen and water vapor would be determined by measuring the integrated Q-branch scattering signals through narrow bandpass filters in front of photomultipliers. The temperature would be determined by comparing the signal from a single hydrogen rotational Raman line to the total hydrogen Q-branch signal. The rotational Raman line would be isolated by a monochromator and detected with a PMT.

Enhanced OH flow tagging, by photodissociation of water with a focused uv excimer laser beam, is being investigated for SSME exit plane velocity measurements. Laboratory H_2/air flames are being

used to simulate exit plane composition and temperature. Spatial and temporal resolution of fluorescence from the enhanced OH zone induced by a time delayed dye laser was investigated with vidicon and photomultiplier detectors. Narrowband uv filters were used to isolate the OH fluorescence signal. A precise timing reference is obtained from OH fluorescence induced by the initial photodissociation process.

The experimental investigation of the feasibility of gas temperature and major species concentration measurements are described together in a section entitled Investigation of Ultraviolet Raman Scattering for SSME Exit Diagnostics. Following that is a section entitled Velocity Measurement with Enhanced OH Flow Tagging which describes experimental studies of velocity measurements for the SSME.

CONCEPTUAL DESIGN INVESTIGATIONS

This section describes the selection of techniques for flow property measurements. Discussion of the relevant techniques is divided between velocity measurements and measurements of temperature and species concentration, because of the similarity of the measurement techniques. The measurement approaches considered and the selections made, are described after a brief introduction describing the flow conditions relevant to the SSME exhaust. The material in this section is based on an informal report on the conceptual design that was prepared by UTRC at the conclusion of Phase I – Feasibility Studies in 1987. As such it is more indicative of the state of the art at that time, rather than at the present.

SSME Exit Flow Conditions

With continued improvements and upgrades planned for the SSME, it would be beneficial to have a diagnostic system capable of measuring pertinent flow variables, such as temperature, species concentrations and velocity. A map of these variables measured in a plane at the exit of the engine would be invaluable for anchoring engine performance codes, or for monitoring the performance of individual engines. It is not likely that physical probes can provide these data because of questions of survival in the hot, high velocity exhaust stream, and because of perturbations such probes cause and the associated problem of correcting data for these effects. For these reasons, a nonintrusive measurement technique is desirable.

To estimate the performance of the conceived diagnostic system, the flow conditions at the nozzle exit plane were taken from the results of TDK code calculations supplied by Klaus Gross (NASA/Marshall). These calculations indicate that the flow at the exit plane is composed of 76.2 mole percent water vapor and 23.6 mole percent molecular hydrogen. Atomic and radical species concentrations such as OH, H, O and H_2O_2 are below 100 parts per million. The calculated static pressure distribution at the exit, shown in Fig. 1, varies from about 0.5 psia on the centerline to 5.5 psia at the nozzle wall. Figure 2 shows the calculated gas temperature varies from 850 K (1600R) on the centerline to about 1400K (2660R) at the wall. The calculated velocity is nearly constant at 4700 meters/second, as shown in Fig. 3. The concentration of major species, H_2O and H_2, are calculated to be essentially constant across the nozzle exit. The concentration profile of the diagnostically important OH radical in the nozzle core flow, calculated by the TDK code, is shown in Fig. 4.

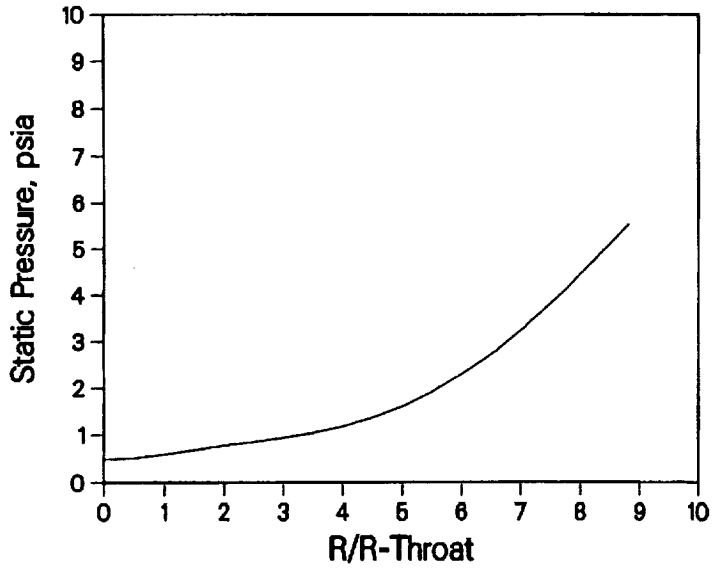

Figure 1. Static pressure at the exit of the SSME calculated with the TDK code.

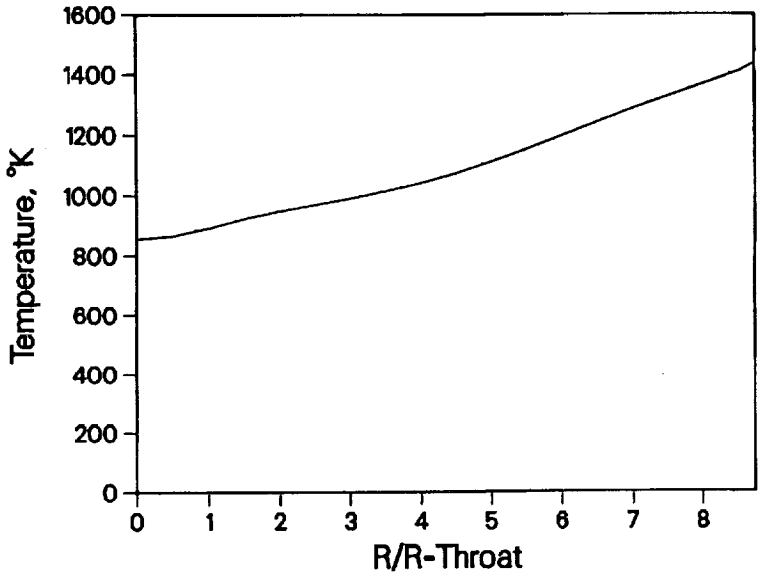

Figure 2. Gas temperature at the exit of the SSME calculated with the TDK code.

Temperature and Species Concentration Measurement Techniques

A number of possible approaches for concentration and temperature measurements were considered in an initial screening. Traditional approaches using absorption or flame emission were rejected because they are hampered by poor spatial resolution and require a plume flow model to interpret results. Laser fluorescence was rejected because the major species in the flow are not

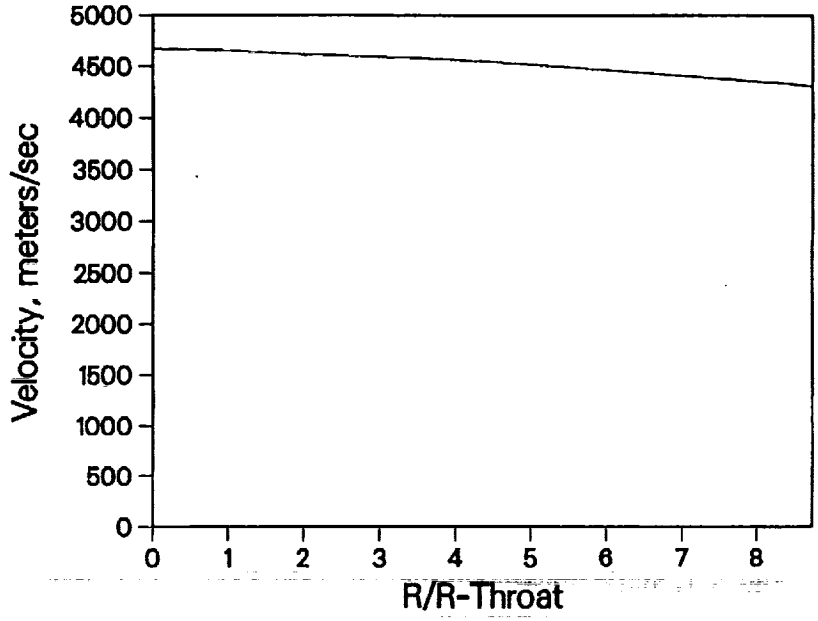

Figure 3. Gas velocity at the exit of the SSME calculated with the TDK code.

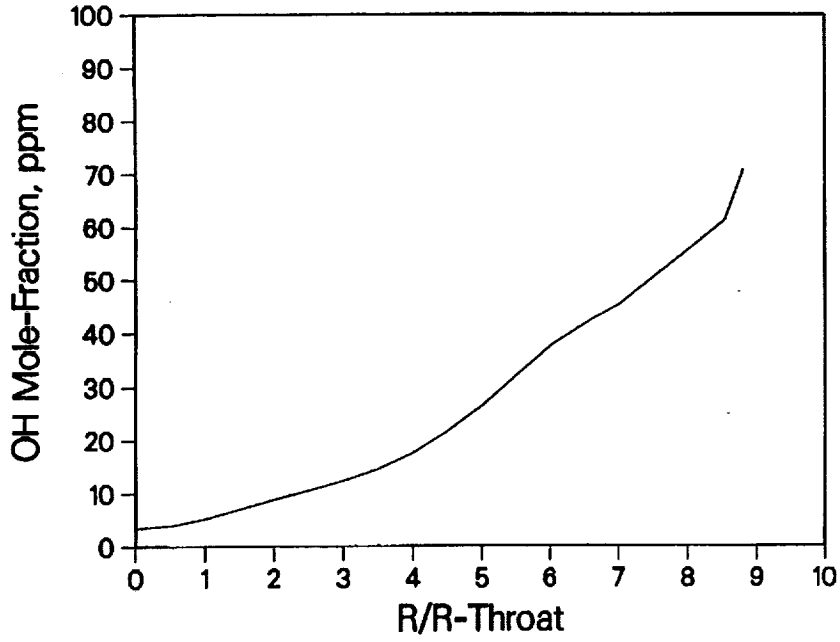

Figure 4. OH radical concentration at the exit of the SSME calculated with the TDK Code.

amenable to excitation by single photon absorption and a separate, tunable laser would be necessary for each species. Rayleigh scattering is not species specific. Both Raman scattering and CARS, however, appear to be capable of temperature and species concentration measurements in the SSME exhaust with available hardware (laser, detectors, etc.).

Raman scattering (RS) possesses a larger number of advantages: (1) ability to interrogate more than one species simultaneously, (2) requirement of a single laser excitation source (3) straightforward analysis of spectral data used to determine species concentration and temperature. On the other hand, RS is a weak process which requires relatively large collection optics near the SSME exit. To permit measurements at the low densities of the nozzle exit, a laser operating in the ultraviolet (KrF excimer for example) must be employed to take advantage of the λ^4 scaling of the Raman scattering cross section to increase the small scattering cross section typical of visible wavelengths.

The advantage of CARS is that it generates coherent (beam-like) radiation that can be efficiently collected. CARS is a wave-mixing process, and two or more lasers are required. For the same reason, however it is necessary for several excitation beams to coincide in the measurement volume – which can be difficult in large scale, turbulent flows. CARS is also nonlinear; the signal generally depends on the molecular density squared. For this reason CARS signal generation is less efficient at low pressures as in the SSME exhaust flow. The calculation of synthetic CARS spectra, which is the basis for data reduction, is complicated by the nonlinearity. Generally a knowledge of the laser frequency profile is needed as well as molecular linewidths. The sparse spectrum of H_2 also presents problems for single-shot measurements due to dye laser spectral noise. The species densities expected at the SSME exit suggest that CARS concentration measurements would require absolute intensity measurements, because interference effects would be too small for accurate measurements from CARS shapes (Hall and Eckbreth, 1984). The main disadvantage of CARS, however, is that it nominally measures one species at a time, except when dual broadband techniques are used (Eckbreth and Anderson, 1985). The gas density at the SSME exit is probably too low for such measurements to be practical.

For the reasons just cited, laser diagnostics based on Raman scattering were selected for temperature and species concentration measurements. The use of the diagnostics is now considered in more detail.

Temperature Measurement Approach

Before temperature and concentration measurement strategies are discussed, the Raman spectra of these molecules should be described. CARS spectra would have the same general features, but with a somewhat different distribution and background structure. The Raman spectra of both of these molecules are composed of a series of strong pure rotational transitions and strong, combined vibrational-rotational transitions. The vibrational-rotational spectra are dominated by $v = 0 \rightarrow 1$, $\Delta J = 0$ transitions, referred to as the Q-branch fundamental band. The calculated vibrational-rotational Raman spectra of H_2O and H_2 are compared in Fig. 5 at 5 psia and T = 800, 1000, 1200 and 1400 K, respectively. Water is represented by the rich spectrum, on the left, composed of many rotational transitions. Hydrogen, because of its small moment of inertia displays only a few rotational transitions. Most of the peaks in the hydrogen spectrum represent transitions from the ground vibrational state to the first excited state. Some weaker 'hot band' peaks, representing $v = 1 \rightarrow 2$ transitions appear in the H_2 spectrum near 3900 cm^{-1}. Hot bands also appear in the H_2O spectra near 3550 cm^{-1}. These correspond to combination and higher fundamental band transitions.

Strategies for determining temperatures Raman scattering measurements are enumerated in Table 1. In this temperature range the first two techniques are the most attractive. The first technique

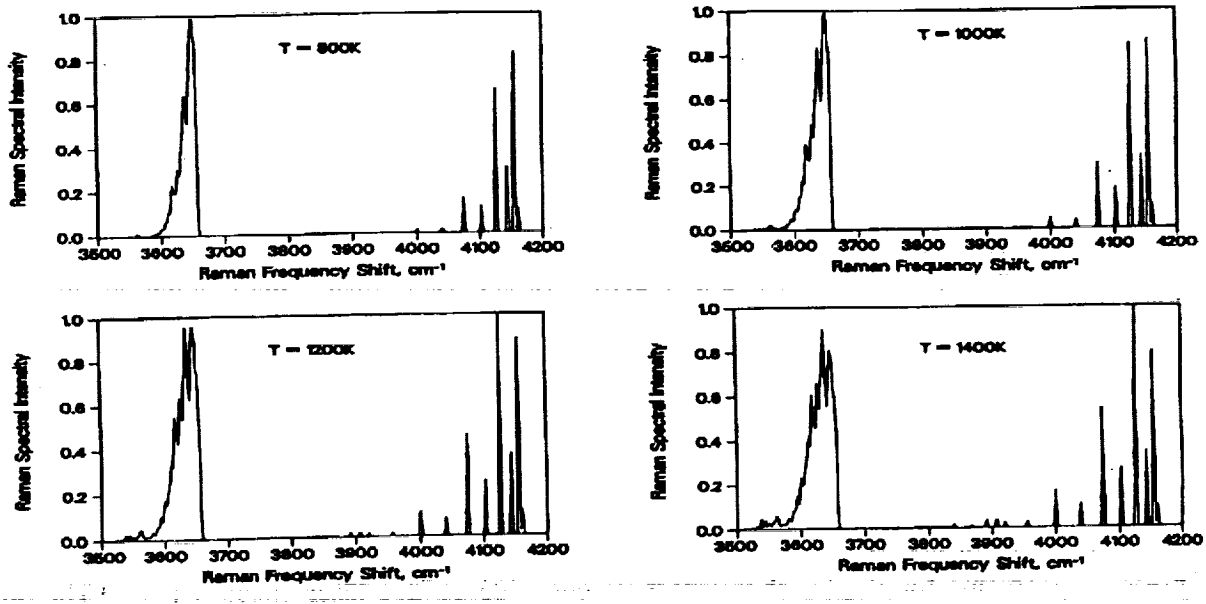

Figure 5. Calculated Raman spectra of H_2 and H_2O for T = 800, 1000, 1200 and 1400 K, for typical SSME exit conditions: 5 psia, 3.0 cm^{-1} slitwidth.

Table 1. SSME Raman Temperature Approaches

- H_2 Q-Branch Distribution
- H_2 Σ S(J $\geq$ 5) to Σ Q-Branch
- H_2 Anti-Stokes to Stokes
- H_2O Distribution
- H_2O Hot/Cold Ratio

uses the distribution of the rotational components in the H_2 spectrum, an approach identical to that taken for temperature profiling in the SSME fuel preburner (Shirley, 1986). The entire resolved spectrum is measured and the contribution of peaks corresponding to different rotational levels is integrated and normalized to recover the Boltzmann distribution, from which the temperature is readily deduced. This approach is ideally the best as interferences can be readily identified and corrected, however the spectrum must be dispersed with a spectrograph and detected by a multichannel detector, which involves losses. Scanning the spectrum would be too slow for Raman scattering in this application.

A simpler approach, in terms of the required equipment, uses filters to select portions of the hydrogen spectrum. The entire H_2 Raman spectrum is shown in Fig. 6. Pure rotational transitions are shown on either side of the laser excitation (zero shift) frequency. Transitions in which a molecule is promoted to a higher energy level by scattering are shown as positive values of frequency shift. These are referred to as Stokes transitions. When an *excited* molecule scatters a photon, it can be de-excited losing its energy to the scattered photon. These are referred to as anti-Stokes transitions. The

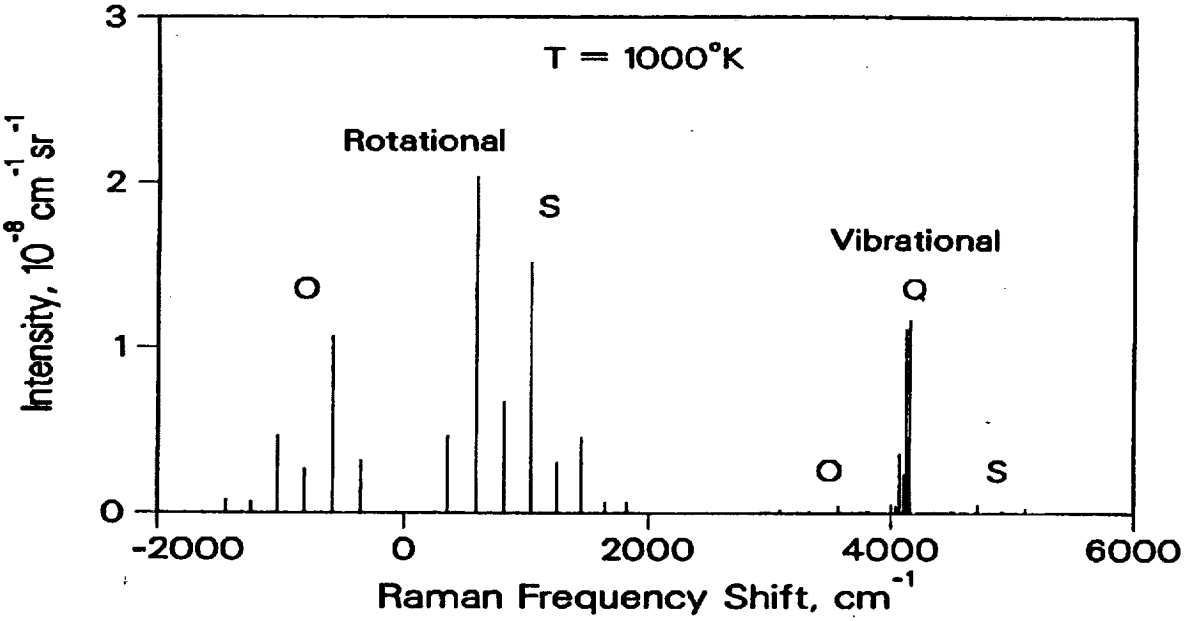

Figure 6. Calculated Raman spectrum of H_2 showing rotational O and S branch and the vibrational O, Q and S branches.

Q-branch on this scale appears compressed. The second technique, then is to compare the temperature-sensitive rotational S-branch transitions ($\Delta J = 2$) to the total Q-branch. This approach requires simpler equipment, potentially affording lower system costs, more rapid data reduction and higher data rates. Figure 7 shows calculated integrated intensity ratios based on the

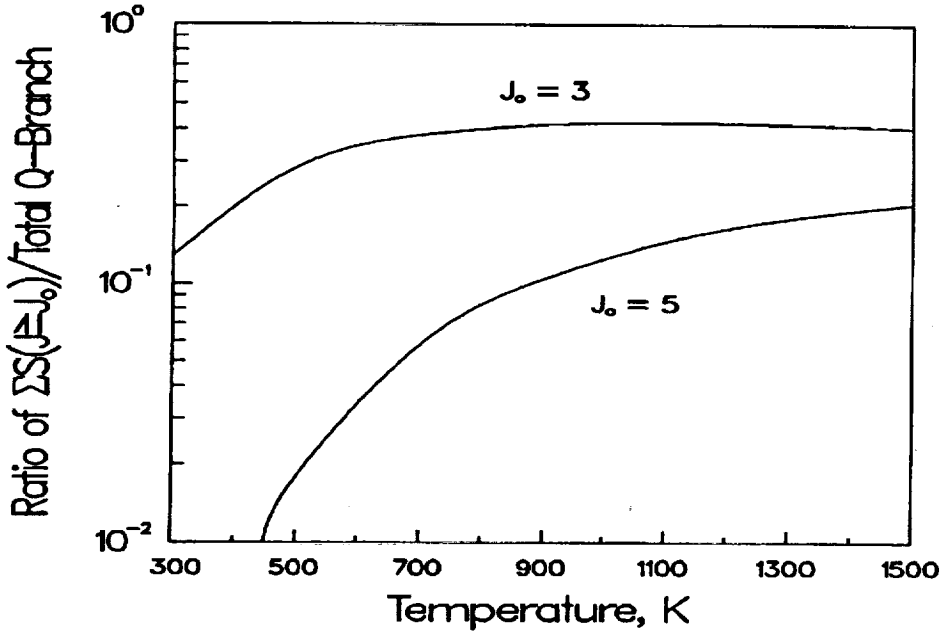

Figure 7. Calculated ratio of the intensity of selected individual rotational transitions compared to the total Q-branch in hydrogen.

measurement of two different sets of rotational transitions as a function of temperature. These calculations show that measurements with the band of S($J \geq 3$) rotational transitions are not sensitive enough at T > 600 K while the band of S($J \geq 5$) transitions has good sensitivity throughout the SSME exit temperature range. These transitions can be isolated with narrow band uv interference filters. Temperature analysis of data would consist of comparing the S- to Q-branch ratio to a calibration using the filter/detection system combination.

The next temperature approach would use the sensitivity of the anti-Stokes transitions to temperature in a ratio measurement, in which the anti-Stokes vibrational transitions are measured with respect to the corresponding Stokes transitions. Calculated anti-Stokes-to-Stokes Q-branch ratios are shown in Fig. 8. Unfortunately, for hydrogen the intensity ratio remain small throughout the expected measurement range, making the technique very sensitive to noise on the anti-Stokes channel, a fact that could be critical if the signal is low. The use of the rotational branch in a ratio measurement does not possess the desired sensitivity, as shown by Fig. 9.

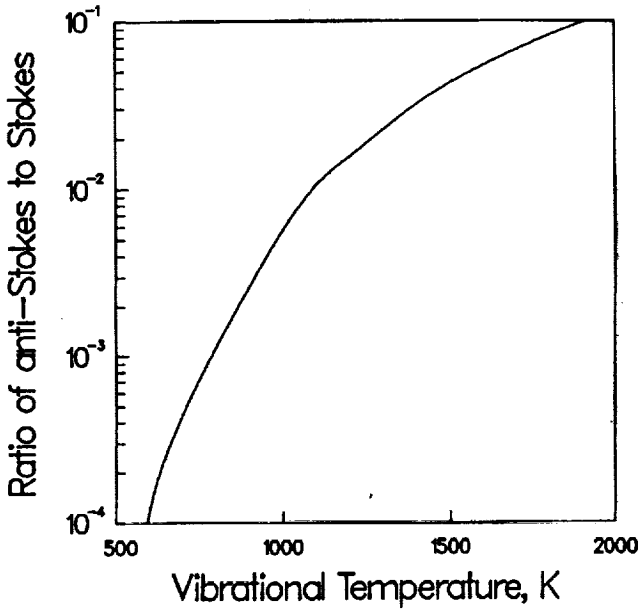

Figure 8. Calculated ratio of the anti-Stokes to Stokes vibrational band intensities in hydrogen as a function of temperature.

The remaining temperature approaches utilize measurements of the Raman spectrum of water vapor. This approach is somewhat jeopardized by lower accuracy of the database of the frequencies of water transition between the higher rotational levels, which are important at the SSME exhaust temperature, and by a limited database of water vapor linewidths (Rahn and Greenhalgh, 1986), which are more important for CARS measurements. The water spectrum contains so many more transitions, that analysis would be slower than with hydrogen spectra.

Concentration Measurement Approach

Concentration measurements can also be made from the strength of Raman scattering, using filters to isolate the water vapor and hydrogen Q-branches at 3657 and 4155 cm^{-1} Raman shifts,

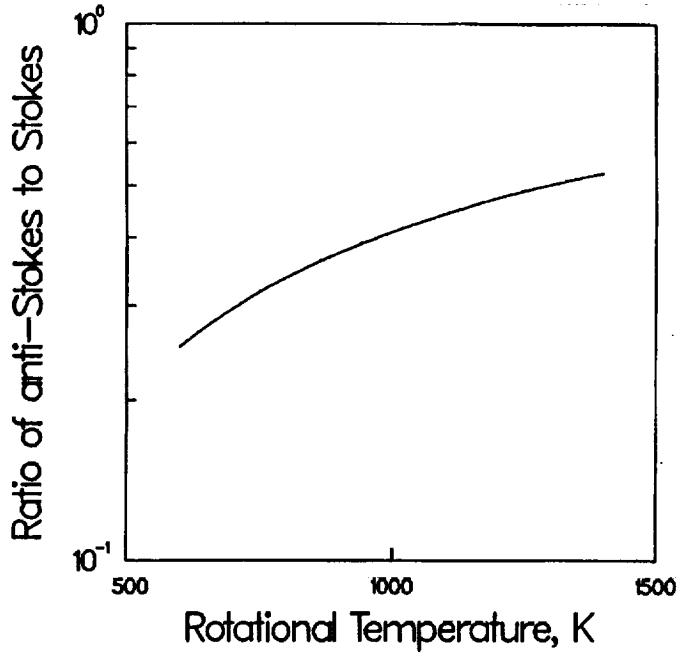

Figure 9. Calculated ratio of the anti-Stokes to Stokes rotational band intensities in hydrogen as a function of temperature.

respectively. Concentration measurements would use some of the same data channels as the selected temperature measurements. These measurements generally require a knowledge of the integrated powers of the measured species as a function of temperature. The integrated power varies directly with the gas density, and therefore inversely with temperature. An additional scaling factor, due to the excitation of higher vibrational transitions such as $v = 1 \rightarrow 2$ which have a larger transition moment, increases slightly with the temperature and is frequently referred to as the vibrational quantum effect. The vibrational quantum effect is very small over the SSME exit temperature range since water and hydrogen have large vibrational energy quanta. The fortunate implication is that concentration measurements can be made independently of temperature measurements.

Absolute concentration measurements would require careful characterization and calibration of the optical system. In particular, the collection volume and the collection solid angle must be determined from simulation experiments. In addition, the system response must be known through calibration with a known source to measure the collection efficiency, the photomultiplier response and amplifier gain. Furthermore, care must exercised to avoid the collection of spurious signals due to inadvertant reflections or undesired scattering. Corrections are also required if the signal transmission is reduced, such as by condensation clouds or particle mists.

Note should be made that even though the mole fractions of H_2 and H_2O differ by a factor of three, the calculated Raman intensities are comparable over the range of 800 to 1400 K. This fortuitous circumstance suggests that Raman measurements of these two molecules will have a good dynamic range.

Raman Performance Calculations

Detailed calculations of the Raman spectra of H_2 and H_2O were undertaken to provide a basis for the comparisons required for temperature and concentration analysis. The Raman signal was calculated for a state-of-the-art KrF excimer laser with 200 mJoule/pulse output at a repetition frequency of 250 Hz. This particular unit is an oscillator/amplifier in which the grating-tuned oscillator injection locks the amplifier to narrow the output bandwidth to 0.001 nm. Without this narrowing, the individual transitions of the H_2 Q-branch excited by the excimer laser would not be resolved. The Raman signal for species i in photoelectrons N_{eR} is given by

$$N_{eR} = \frac{P_L t \left(\frac{d\sigma}{d\Omega}\right)_i n_i \varepsilon_c \eta_Q \ell \Omega}{hck_s}$$

where P_L is the laser power, t the signal collection time, $d\sigma/d\Omega$ is the Raman cross-section, n_i is the species population density, ε_c is the collection efficiency, η_Q is the detector quantum efficiency, and hck_s is the Raman (Stokes) photon energy. ℓ and Ω are respectively, the spatial resolution and collection solid angle. The collection efficiency of a receiver system composed of optical filters and reflective optics is estimated to be about 8 percent, principally due to the low transmission of uv narrowband filters. The quantum efficiency of bialkali photomultiplier tubes is near maximum for any photocathode, 25 percent. ℓ and Ω are the most critical experimental parameters. They are not independent for a backscattering configuration, which would be most practical for this application. Both parameters are determined by the system f/number, $N{:}\Omega = \pi/(4N^2)$ and $\ell \cong 2 f \theta N$ where f is the collector focal length and θ is the laser beam divergence entering the focusing optics, which is assumed to be the same focal length as the collector.

The total H_2 population density, n_i varies from 0.7×10^{17} cm^{-3} at the center of the exhaust flow to 4.5×10^{17} cm^{-3} at the edge. The experimental parameters required can be evaluated by substituting values ($d\sigma/d\Omega = 3 \times 10^{-29}$ cm^2/sr, $hck_s = 7.2 \times 10^{19}$ J) in equation 1 and rearranging

$$P_L t \ell \Omega = 1.2 \times 10^{12} \frac{J.sr}{cm^2} . \frac{N_{eR}}{n_i}$$

Figure 10 shows how the factor on the right hand side varies across the exit. To make a temperature measurement with ±30 K precision requires the collection of about 10,000 Raman photoelectrons (Shirley, 1986). Considering different spatial resolutions, the incident laser energy, $P_L t$, to achieve this temperature precision can be calculated. This comparison is shown in Table 2, in which a focal length of 6.7 m (22 feet) has been assumed, similar to the OPAD measurements. It is seen that at 10 cm resolution, almost 5 J or 25 laser pulses, corresponding to an integration time of 0.1 second, are required to make a measurement at the edge, while nearly 150 pulses (0.6 seconds) are required at the center. When a larger collector (35 cm) is considered a spatial resolution of 5 m is predicted and 2.5 J or 13 shots are required for a measurement at the edge of the flow. A single shot measurement is estimated to have an uncertainty of ±80 K for this size collection optic.

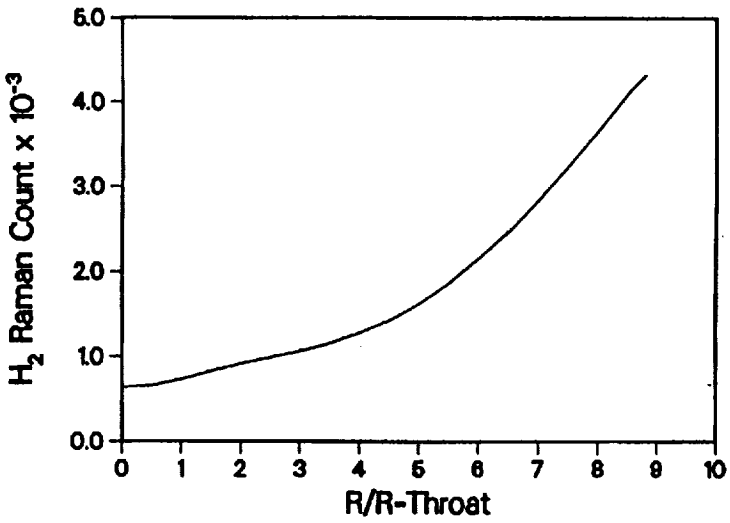

Figure 10. Calculated Raman signal levels as a function of radial position at the SSME exit for E_L = 5 J, L = 5 cm and Ω = 0.0022 millisterdian.

Table 2. H_2 Raman Temperature Measurement Laser Energy Requirements

$\Delta T = \pm 30K$

Spatial Resolution	f/number (N)	Collector Diameter	Laser Energy, Pt	
			edge	center
5	19	35	2.5	16
10	37	18	4.7	30
15	56	15	7.1	45
(cm)	–	(cm)	(J)	(J)

Interferences

Possible interferences to KrF laser-excited Raman measurements have been considered as a function of the Raman shift from the excitation wavelength. At small Raman shifts, 200-600 cm^{-1}, the pure rotational Raman spectrum of H_2O interferes with the pure rotational Raman hydrogen spectrum and may potentially perturb the selected temperature measurements. Measurements have not been made at temperatures higher than 430 K (Murphy, 1977). It is not likely, though, that water transitions will pose a problem for measurements at the large (1447 $cm^{-1)}$ shift of the S(5) transition of the H_2 rotational Raman spectrum. The Q branches of H_2 and H_2O can be separated with carefully specified filters. Flame emission from OH may pose a problem. Measurements at the SSME exit show strong emission when compared to laboratory measurements at wavelengths less than 305 nm from bands at 270, 275, 285, and 295 nm (Gaydon, 1974). Since this emission is cw it can be discriminated against using gated amplifiers. If the emission background is large enough to saturate the photomultiplier or act as current drain the high voltage can be gated as well. The question is how the intensity of these transitions compares with the pulsed Raman intensities and whether the 30 ns gate of Raman measurements (or longer considering the PMT pulse spreading) provides sufficient discrimination in averaging over 0.1 second time periods.

Possible laser-excited OH fluorescence could be a more difficult interference to the discrimination of Raman signals. The most likely mechanism that can be conceived is photodissociation of H_2O and excitation of OH by two-photon absorption of the 249 nm laser radiation. This process is discussed later in more detail in the section of this report on velocity measurements. This interference was characterized in laboratory measurements described later in this report. In general, the OH population levels in the core flow are low enough that this interference is not important. Interference from laser induced fluorescence from oxygen can also be a problem, but nominally only in regions where the oxygen exists, such as the shear layers which entrain ambient air at the edge of the exhaust plume.

The question of potential interference from background solar radiation has been examined. The filters used to isolate the desired uv Raman-shifted bands are limited to a relatively broad (30-50 Angstroms) bandwidth. This permits a portion of the solar uv spectrum, in the region strongly absorbed by atmospheric ozone, to pass through the detection optics. Unless the horizontally mounted receiver is pointed directly at the sun (sunrise, sunset) or viewing glint, the background sunlight radiance arises from indirect radiation, i.e. skylight. An estimate can be made from Bell, *et al.*, (1960) of the sunlight spectral irradiance - 0.1 to 1.0 $mW/cm^2-sr-\mu m$. The Raman system would collect light from 1 cm^2 with a collection solid angle of about 1 millisteradian. A 50 Angstrom filter bandwidth corresponds to .005 μm. The detected radiated power due to sunlight is 5×10^{-9} W, which corresponds to 7×10^9 photons/sec. If the gated integrator has a 30 nsec gate, it is estimated that 210 photons of background sunlight will enter the collection system. This is four orders below the Raman signal. The background count due to sunlight is reduced still further by collection and quantum efficiency factors so that even without light shields, it is probably negligible under normal circumstances. Again, gating of the PMT voltage can be used to minimize current drain.

A severe problem revealed by the optical plume anomaly detector (OPAD) tests is caused by the water sprayed into the flame deflector bucket on the engine test stand. When the prevailing wind blows the plume back towards the test stand, it causes a large attenuation in OPAD detection channels. UV Raman measurements would be similarly affected. This would yield a large data drop out for these measurements. It would be desirable to operate only when the prevailing wind blows in the direction of the deflector flow.

Velocity Measurements

The environment associated with SSME testing presents difficulties for velocity measurement. These difficulties include the plume, acoustic noise, vibration, spurious water vapor clouds entering the viewing path, and startup and shutdown transients. In addition, a large amount of accurate velocity information must be acquired during tests which will last, at most, a few minutes. Standard Laser Doppler Velocimetry (LDV), with seeded or naturally occurring particles, is precluded by the pure cryogenic fuel and oxidizer conditions, severe combustion conditions, hardware component sensitivity, high flow rate, and nonsooting nature of the flow. The state of art for alternative velocity approaches is limited, partly because of the success of LDV over the last 10-15 years. A few approaches had been identified prior to the start of this study, but these required further examination to determine if they were promising, even from a qualitative viewpoint, for the SSME exit plane.

Measurement Approach

As a result of these difficulties it was important to establish clearly a few key simplifying assumptions. Then a general search could be conducted to identify a broad group of potential SSME exit plane velocity approaches. From this group several promising approaches for the SSME exit plane would be selected, if possible, using a set of qualitative criteria. These promising approaches would be evaluated and compared on a quantitative basis. The results of this comparison would then be combined with a review of the key assumptions prior to formulation of final conclusions and recommendations. The assumptions are given below.

Assumptions

1. The flow is essentially parallel and steady after startup. Measurement of a single, time-averaged, velocity component parallel to nozzle axis is to be considered.
2. Seeding of particles or trace species (I_2, Na) is precluded by the nature of fuel, oxidizer, combustion, and flow conditions, and also by hardware component sensitivity to foreign matter.
3. Approaches must utilize naturally occurring species (H_2O, H_2, OH) or properties (density).
4. Vibration levels and optical interface conditions with the SSME will be acceptable.

Potential Velocity Diagnostic Approaches

The SSME exit plane conditions and environment are shown schematically in Fig. 11 for sea level operation. Conditions at the exit plane were obtained from the TDK solutions discussed earlier. Both wall boundary layer and core flow profile measurements at the exit plane are desired. Accurate thrust and specific impulse values are known for SSME. In order to contribute to future improvements in performance, core flow average velocity measurements should be made to a precision of about 1 percent. Plume boundary, boundary shock, and Mach disk contours and locations are based on information provided by Terry Greenwood of the Plume Group at MSFC (Smith, 1980).

The wake, shear layer, and boundary shock information shown in the enlarged view of the wall in Fig. 11 represents a qualitative model we have developed, since the detailed structure of this region has not been of interest in plume studies. The wall boundary layer shown represents displacement thickness, about 6-7 mm, calculated as part of the TDK solutions. The velocity boundary layer would be 2-3 times as large, at about 25 mm at the 10 % velocity deficit point, as shown in the model results provided by Terry Greenwood (Audeh, 1974). These latter results indicate that very close to the wall, about 1 mm, the velocity deficit increases to 40%, and the flow should still be supersonic, since temperature has not changed much. Hence, most of the velocity boundary layer flow outside 1 mm should persist a short distance beyond the exit plane before encountering the boundary shock. Further quantitative model results about the flow field near the wall would be helpful. Velocity measurements in the boundary layer region of 1-5 percent precision would be valuable. Available information (Gross, 1987) indicates that the concentration of H_2O will remain high throughout the boundary layer, and is relatively unaffected by addition upstream of hydrogen to cool the wall.

A broad group of potential velocity diagnostic approaches was developed, consistent with the above assumptions, to address the SSME exit plane conditions. All potential velocity approaches

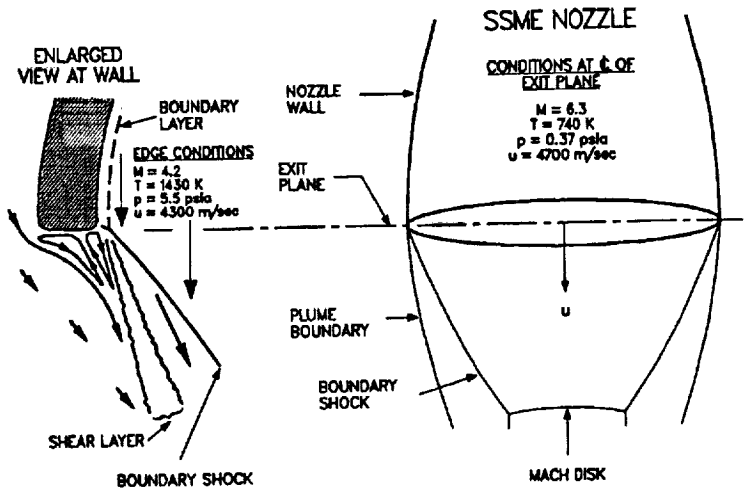

Figure 11. SSME external flow and enlarged detail of the model flow at the nozzle lip showing mixing of the nozzle flow with the entrained ambient flow.

considered are listed in Table 3, together with qualitative criteria for application to the SSME exit plane. Seven potential velocity measurement approaches are shown in Table 3. They are Rayleigh–Doppler, fluorescence–Doppler, uv photodissociative–tagging or Doppler, schlieren/ photothermal–tagging, RELIEF–tagging, stimulated Raman–Doppler, and CARS–Doppler. A brief discussion of each potential approach and its application to SSME is given below.

Table 3. Characteristics of Velocity Measurement Approaches for SSME Exit Plane Application

Techniques	Accuracy (Prelim.)	Range	Applicability[1]		Complexity	Uncertainties
			core flow	boundary layer (BL)		
• Doppler-Rayleigh	high <1%	point	A	A	moderate	spurious luminosity and line profile
• Doppler-fluorescence	moderate 1-5%	point & 2-D	?	?	moderate	natural OH concentration
• photo-predissociative (tagging or doppler)	moderate 1-5%	2-D or point	A	A	moderate	predissociation of H_2O to OH; OH decay
• schlieren/photo-thermal (tagging	moderate 1-5%	point 2-D	A	?	moderate	plume effects:vibration
• RELIEF[2] (tagging)	moderate 1-5%	2-D	?	?	moderate	interogation:2-photon or 2-D CARS: H_2 (V) decay
• Doppler-stimulated Raman	moderate 1-5%	point	?	?	high	plume effects and angle; signal strength
• Doppler-CARS	moderate to high	point	A	?	high	plume, angle

1. A = applicable, need more details; ? = perhaps, need to resolve uncertainties
2. Raman excitation + laser induced electronic fluorescence (RELIEF)

Rayleigh-Doppler

Light scattering in a gas for which the frequency remains essentially unchanged is known as Rayleigh scattering (Landau and Lifshitz, 1960). The internal energy state of the gas molecule does not change and overall energy change is only the very small amount required to conserve momentum in the photon-molecule collisions. The overall scattering is incoherent, due to the disordered thermal motion of the molecules (Fabelinski, 1968). Rayleigh scattering occurs because of spatial and temporal inhomogeneities within the scattering volume that are referred to as fluctuations. When the mean free path of the molecules is large compared to the light wavelength then gas collisions are not important and the scattering occurs independently at each molecule. In this case the Rayleigh scattering spectrum from a laser line approaches the broad Doppler line shape of a Gaussian (Yip, 1970). At high enough pressure however, gas collisions become important, and the Rayleigh scattered spectral shape will change due to density fluctuations that propagate as thermal waves. An effect

occurs known as Brillouin scattering, which causes wings to appear in the scattering spectrum, as described in the above references. Brillouin effects however turn out to be relatively unimportant for the SSME exit plane, as discussed below.

The Doppler-broadened line profile of Rayleigh scattered light from a single-mode argon ion laser has been measured in a flame (Cattolica, Robben and Talbot, 1976). They showed that Brillouin scattering was not significant in temperature measurements performed in a one atmosphere pressure premixed hydrogen-air flame from the Rayleigh scattered spectral profile. The profile was measured with a computer controlled Fabry-Perot spectrometer. As noted by Cattolica, *et al.* (1976), the spectral structure of Rayleigh scattering has not been exploited with regard to velocity or temperature. One can only speculate that the high degree of success of the conventional approach, laser Doppler velocimetry (LDV) with particles, has been partly responsible. Also in practical systems, the Rayleigh scattering will often suffer badly from Mie interferences and spurious scattering.

Conditions in the SSME exit flow however, are favorable for consideration of Rayleigh-Doppler methods to measure an average gas velocity with a narrowband pulsed laser. These conditions include low luminosity, only occasional spurious particles, significant pressure but less than one atmosphere, and high gas velocity. Accuracy with Rayleigh scattering may be high, since the reference line is the laser line, which can be narrow. Since the scattered line is broad, the detector would probably be a high finesse scanning Fabry-Perot spectrometer, rather than a heterodyne process. The application of heterodyne detection in such cases is not necessarily ruled out, but requires further study and clarification.

Fluorescence-Doppler

Fluorescence-Doppler in the SSME case pertains to excitation of electronic fluorescence from naturally occurring levels of the OH radical in the exit flow. Doppler-shifted absorption/fluorescence detection, utilizing a narrowband tunable dye laser, would allow acquisition of velocity information without having to detect OH fluorescence through a Fabry-Perot. Point or 2-D velocity measurements are possible by using point or sheet illumination with the narrowband laser. In conventional Doppler fluorescence, a wider bandwidth laser would be used to excite an OH transition over its entire absorption line profile. In this case, point velocity data are obtained by viewing OH fluorescence through a Fabry-Perot at two angles to the flow, or at one angle and in a reference cell.

For both these Doppler methods, the main uncertainty is the level of OH in the exit plane. Equilibrium OH concentrations are too low and nonequilibrium effects would have to be significant. Finite rate, 2-D kinetic analysis results from the TDK code, Fig. 4, indicate OH mole fraction levels of about 3×10^{-6} (3 ppm) at the centerline. This would correspond there to an OH concentration of about 1×10^{12} cm^{-3}. Detectivity of OH in laboratory experiments (Lucht, *et al.*, 1983) is $10^{12} - 10^{13}$ cm^{-3}, depending on averaging time, spectral and spatial resolution. Hence naturally occurring levels of OH at the centerline may be too low for practical use as a velocity diagnostic species. At the edge of the wall boundary layer, TDK results (Fig. 4) show OH increasing to about 80×10^{-6} mole fraction (80 ppm), which may be useful for diagnostics.

Doppler-shifted absorption/fluorescence velocity measurements in gas flows have been made extensively by Hanson and his group at Stanford (McDaniel, Hiller and Hanson, 1983) (Hiller and

Hanson, 1985) utilizing iodine vapor as a trace additive, and a 2-D optical multichannel detector, for 2-D velocity imaging. Doppler-shifted viewing of fluorescence through a Fabry-Perot spectrometer has been utilized in numerous studies, using either natural line emission, such as occurs in plasma flows (Bohn, Beth and Nedder, 1967), or line emission induced by an electron beam (Becker, Robben and Cattolica, 1973). To our knowledge, Doppler-shifted OH velocimetry has not been demonstrated.

UV Photodissociative-Tagging or Doppler

Photodissociation of water, $H_2O + h\nu \rightarrow H + OH$, with a uv excimer laser has been considered as a means of locally enhancing the OH concentration in the exit plane. Single photon and two photon processes are being examined for available uv excimer laser wavelengths of interest, principally ArF at 193 nm, and KrF at 248 nm. The initial production of OH is discussed here. Subsequent decay of OH for SSME conditions is considered in a later section of this report.

Considering single photon processes, the ArF line is very close to the edge of the first photon absorption band of room temperature water, which has a classical limit at about 186 nm (Watanabe and Zelikoff, 1953). This absorption band extends to about 140 nm and is now known to be due primarily to dissociation which produces OH in the ground electronic state and H (Andresen, Ondrey and Titze, 1984). Fluorescence from OH does not occur, only production. Based on energetics, it appears reasonable that H_2O in its first vibrational state will extend the absorption band to include the ArF line. At edge flow conditions, 1430 K, a significant amount of the first excited stretching mode of H_2O will be populated (about 2.3 mole-% or 23000 ppm). This could represent the source of controlled excitation of a significant level of OH for flow tagging using the ArF line. Experimentally, significant absorption of an essentially unfocused ArF excimer laser beam at 193 nm has been reported in the postflame region of a premixed methane flame (Chou and Dean, 1985). They measured significant enhancement of OH concentrations, which they attributed to hot band absorption in H_2O.

Two photon excitation of H_2O with a KrF excimer laser at 248 nm was investigated by Fotakis, McKendrick and Donovan (1981). The two photon process energetically involves photodissociation at 124 nm, which is within the second absorption band of water (Watanabe and Zelikoff, 1953) (Andresen, Ondrey and Titze, 1984), and can produce electronically excited OH and result in fluorescence. A line-narrowed, tunable, KrF laser has been used in other studies (Hodgson, *et al.*, 1984) to investigate in more detail the steps leading to production of electronically-excited OH. In general, the electronically excited OH molecules are born in very high rotational states. Resonance enhanced multiphoton ionization of H_2O to H_2O^+ at 248 nm by a (2+1)-REMPI process has been observed in recent work by a group including Andresen (Meijer, *et al.*, 1986). They have obtained branching ratios for the predissociation, ionization and OH fluorescence processes. The decay of OH fluorescence generated by this two photon process has been studied by Papagiannakopoulos and Fotakis (1985), who estimate their OH production at <1 mole-%. Production of OH and the fluorescence signal strength for SSME conditions will probably have to be based on laboratory experiments with focused 248 nm radiation. Two photon processes with focused ArF radiation at 193 nm have been explored briefly in these reported studies (Fotakis, McKendrick and Donovan, 1981), however, OH fluorescence was not significant and no OH quantitative production level

measurements were attempted. The structure of H_2O near 97 nm apparently is complex and not known well enough.

Schlieren/Photothermal-Tagging

Photothermal velocity diagnostics (Rose and Gupta, 1985) involve precise generation of a density disturbance in the flow at one point and timing the arrival of this disturbance at a later known point in the flow with a quadrant detector. If the schlieren technique is added to photothermal perturbations, then some spurious effects may be minimized in the SSME by the introduction and proper orientation of the knife edge. Detection also changes from time of arrival to tracking. A pulsed tunable IR laser (2-5 μm) could be used to create a selective absorption in water at a precise spatial location. This density disturbance would be tracked, in a schlieren process, over a region illuminated uniformly with a pulsed probe laser, probably a frequency-doubled Nd:YAG at 532.0 nm. The tracking would be done with an OMD. Time-averaged values of the density disturbance location could be acquired at several values of the delay time between the excitation and probe laser beams. The principle difficulty with this approach is that spurious signals are created when the probe beam encounters other fluctuating sources of density and index gradients in the flow field. In the SSME exit plane case the biggest spurious effects may be generated in the shear layer between the ambient air and the plume flow. Temperature and composition fluctuations probably exist in this layer which may be the source of disturbances as large as those which could be created in the flow. Modified schlieren methods exist to locate three dimensional disturbances and discriminate against such spurious effects. These methods create a schlieren system with a finite depth of field by imaging multiple source slits onto multiple knife edges and imaging the desired disturbance with large magnification (Boedeker, 1959). The detector array in that case might have to be rather large.

RELIEF-Tagging

Raman excitation followed by laser induced electronic fluorescence detection (RELIEF) was demonstrated recently by Miles, *et al.* (1987) as a flow tagging diagnostic for oxygen. In the SSME case it would pertain to tracking vibrationally excited hydrogen. A stimulated Raman process would be used to generate a large population of vibrationally excited hydrogen, $H_2(v)$, at a point or along a line. A two photon or a 2-D CARS process would be used in conjunction with an OMD to selectively interrogate this $H_2(v)$ and determine its spatial location after a known delay time. One concern here is the potentially rapid decay of $H_2(v)$ in the presence of large concentrations of H_2O. Specific information on this decay rate, but may not be available for SSME conditions. For detection, it appears that a two photon process could excite electronic states of H_2 , but the subsequent emission may be primarily in the deep uv and subject to strong absorption by H_2O in the flow and ambient air. Secondary emission lines would have to be identified in the visible. The alternative detection process is 2-D CARS, tuned to generate a CARS signal only at the spatial point where the $H_2(v)$ is present.

Stimulated Raman-Doppler

The stimulated Raman gain-Doppler method was developed by Exton and Hillard (1986) in an application to N_2 in a supersonic, continuous flow, air wind tunnel. For the SSME, stimulated Raman would have to utilize H_2. A precise beam overlap focal zone would have to be created in the presence

of plume effects. Stimulated Raman is a double-ended process and must be angled to the flow by less than 90 degrees to introduce a Doppler shift. The angle could be 60-70 degrees from the axis, and the focal zone would be located a s much as 40-70 cm away from the exit plane. The H_2 number density in the core flow is low enough, about 0.002-0.02 relative to STP density, that stimulated Raman signal levels may be marginal. Density of N_2 in the Exton and Hillard case was about 0.1 relative to STP and their scan time was two minutes per point with a 10-20 Hz system.

CARS-Doppler

Velocimetry with CARS for SSME would utilize H_2 and should have more favorable signal levels and background discrimination than stimulated Raman, since the coherent signal is spatially separated from the generating beams. CARS velocimetry has not been studied extensively, but a laboratory demonstration has been reported (Gustafson, McDaniel and Byer, 1981). Since CARS is generally studied as a multiple-beam forward propagating process, one difficulty would be a smaller Doppler effect. In this regard, large angle and counterpropagating CARS phase matching geometries have been reported (Chandra, Compaan and Wiener-Avnear, 1978 and Compaan and Chandra, 1979) which would enhance the Doppler effect. Since the process must be angled and is double-ended, CARS velocimetry also would not be able to measure velocity very close to the SSME exit plane.

Selection of Most Promising Velocity Approaches

The characteristics of the potential velocity approaches, as described above, have been combined with a set of qualitative selection criteria for SSME diagnostics. These criteria are given by column headings in Table 3. They are accuracy, range, applicability, complexity, and uncertainties. Accuracy is based on a qualitative, preliminary assessment of relative signal shapes. For example, with Doppler-Rayleigh, a narrow reference line would be compared with a broadened, scattered line profile, while for fluorescence-Doppler, both reference and signal lines are broadened. Actual accuracy must include quantitative signal/noise estimates, which are made for the selected approaches in the following section. Range refers to whether 2-D as well as point velocity measurements are possible. Applicability refers to whether core and boundary layer regions can be explored. Complexity is a qualitative judgement about equipment requirements and technique feasibility in the SSME environment. Uncertainties refer primarily to points raised in the detailed discussion of each approach in the previous section.

The techniques selected as most promising are Rayleigh-Doppler and photodissociative-tagging or Doppler. This selection is based on the clearest applicability at this time to both core and boundary layer flow regions, on only moderate complexity, and on, perhaps, the least uncertainties.

Comparison of Rayleigh-Doppler and Enhanced OH Approaches

A comparison of the key conditions and quantitative results for the velocity approaches developed in the previous section is shown in Table 4. The approaches are listed in order of complexity of the interrogation laser. In this comparison, it is possible that any of the approaches could shift one way or the other by a factor of two due to uncertainties in the calculational method. Except where

noted, factors of ten differences among the approaches in comparison with SSME requirements are thought to be significant however, and these results should help to identify the approach or approaches that should be considered further.

A key observation from Table 4 is that OH Doppler-Enhanced Fluorescence in the uv is far too slow to be of interest for SSME. By inference the two photon OH Doppler-fluorescence would also be too slow. This is a consequence of low OH concentration, the need to isolate an individual line with a monochromator ahead of the Fabry-Perot (F-P), and of course the need for the F-P to acquire the line profile. Doppler-Rayleigh by contrast is only marginally slow, a consequence of scattering off the total concentration at 532nm and the absence of a special requirement to isolate a line. Therefore the simplest approach, which would only require the excitation laser, will be feasible for SSME when single-mode laser technology has been successfully extended to practical uv excimer lasers operating at 248 nm with 50 W average power. Since the laser does not have to be tuned during a Doppler-Rayleigh velocity measurement, a practical uv system may be possible with a single-mode pulsed dye laser/two excimer laser approach. As discussed earlier this would reduce the data acquisition time for Doppler-Rayleigh by more than a factor of 250.

The best approach to focus on for SSME from Table 4 is obviously OH flow tagging. Flow tagging is significant in large part because of OMD technology, where signal is acquired on all channels for every laser shot. The narrowband-laser, Doppler absorption/fluorescence approach is attractive because the Fabry-Perot is not in the primary detector path. The narrowband laser result shown in Table 4 could perhaps be significantly better because of the conservative nature of the calculation, and this has been indicated by a less-than designation. However, the narrowband (single-mode), pulsed dye laser system would be more difficult to develop since it would have to be tunable and operate at many potential OH wavelengths.

Conclusions and Recommendations for Velocity Measurements

The quantitative comparison of Doppler-Rayleigh and enhanced OH approaches indicate that enhanced OH flow tagging has by far the best data rate potential for accurate velocity measurements. Enhanced OH-Doppler, with a narrowband, tunable, pulsed dye laser, is also of interest – although the dye laser system would be complex. Doppler-Rayleigh appears too slow. This comparison is based on using available commercial lasers that are reliable and of rugged construction. For Doppler-Rayleigh this imposes a performance limit based on wavelength and average power of available single-mode frequency doubled Nd:YAG lasers. The availability of a single-mode, pulsed uv excimer laser would make Doppler-Rayleigh potentially attractive for SSME.

Table 4. Quantitative Comparison of Applicable Velocity Approaches

SSME Exit Plane, Single Point Data, 1% Accuracy
(100 channels, 1000 counts/channel)
1:1 Imaging, 6×10^{-3} steradians, OH = 10^3 PPM

Approach	Excitation Laser Horizontal Beam	Interrogation Laser	Detection	Quantitative Results		
				Spatial Resolution, mm	Acquisition Time, sec	
					centerline	edge
Doppler -Rayleigh	Single-Mode Nd:YAG (532 nm) 0.2 J, 20 Hz	None	Scanning Confocal Fabry-Perot (θ_v = 75°)	1 x 1 x 4	250	30
2 Photon OH Doppler-Fluorescence	Excimer KrF (248 nm) 0.2 J, 250 Hz	None	Spectrometer and Scanning Fabry-Perot (θ_v =71°)	0.1 x 1 x 3	?	?
OH Doppler-Enhanced Fluorescence	Excimer KrF (248 nm) or ArF (193 nm) 250 Hz	Broadband Pulsed Dye Laser	Spectrometer and Scanning Fabry-Perot (θ_v =71°)	0.1 x 1 x 3	10000	1200
OH Flow Tagging	Excimer KrF (248 nm) or ArF (193 nm) 250 Hz	Broadband Pulsed Dye Laser	OMD Linear Diode Array	1 x 1 x 10 x 8	0.4	0.05
Narrowband OH Doppler-	Excimer KrF (248 nm) or ArF (193 nm) 250 Hz	Narrowband Tunable Pulsed Dye Laser (θ_1 = 71°)	Filter/PMT	1 x 1 x 3	<100	<12

INVESTIGATION OF UV RAMAN MEASUREMENT

High average laser power is required to implement temperature and concentration measurements with Raman scattering. Excimer lasers are available operating at 250 Hz with 0.2 J pulse energies at 248 nm (KrF), about 50 W average power, that can satisfy Raman and flow-tagging requirements. Frequency quadrupled Nd:YAG lasers by comparison operate at 10-20 Hz and produce only about 1W average power at 266 nm. For enhanced OH velocimetry, the high repetition rate of the excimer laser is attractive to maximize data rate.

The excimer laser diagnostic system is shown schematically in Fig. 13. The excitation laser and the interrogation laser for OH fluorescence imaging are focused by optics into the SSME exhaust flow. A telescope collects scattered radiation and directs it to separate detection optics for velocity and temperature/species measurements. While it should be possible to shield the excimer and dye lasers from rocket acoustic and vibration effects, it seems more advisable to locate these lasers within the hardened test stand when possible. This is not only because of the large physical size of an excimer laser, but also because of the need to provide gas and vacuum services and vibration isolation for alignment sensitive optics. The details of the setup will depend on available access on the particular rocket engine test stand.

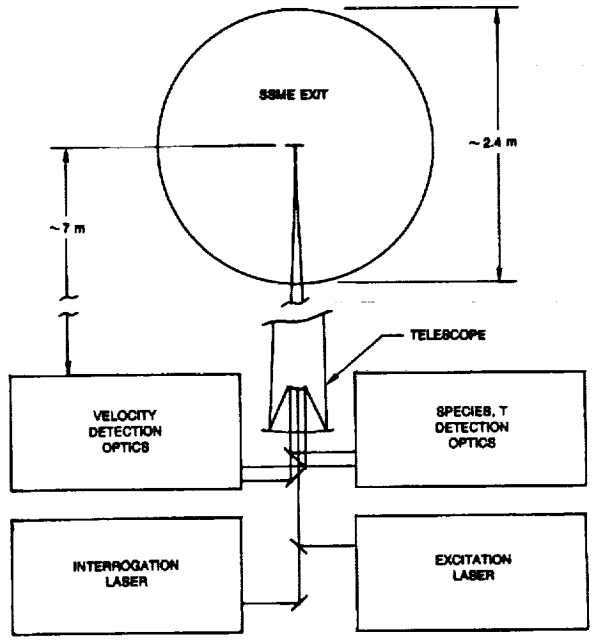

Figure 13. Schematic layout of the SSME exit plane diagnostic instrumentation.

Raman Performance Calculations

Detailed calculations of the Raman spectra of H_2 and H_2O were undertaken to provide a basis for the comparisons required for temperature and concentration analysis. The Raman signal was

calculated for a state-of-the-art KrF excimer laser with 200 mJoule pulse output at a repetition frequency of 250 Hz. This particular unit (Lambda-Physik 160T-MSC) is an oscillator/amplifier in which the grating-tuned oscillator injection locks the amplifier to narrow the output bandwidth to 0.001 nm. Without this narrowing, individual transitions of the H_2 Q-branch excited by the excimer laser would not be resolved, and laser induced fluorescence interferences would arise.

A temperature measurement with ±30 K precision requires the collection of about 10,000 Raman photoelectrons (Shirley, 1992). Considering different spatial resolutions, the incident laser energy, $P_L t$, to achieve this temperature precision can be calculated. This comparison is shown in Table 5, in which a focal length of 6.7 m (22 feet) has been assumed, similar to the SSME plume measurements (Cikanek, *et al.*, 1987). At 10 cm resolution, almost 5 Joules or 25 laser pulses corresponding to an integration time of 0.1 second, are required to make a measurement at the edge, while nearly 150 pulse s (0.6 seconds) are required at the center. When a larger collector (35 cm) is considered, a spatial resolution of 5 cm is predicted and 2.5 J or 13 shots are required for a measurement at the edge of the flow. A single shot measurement is estimated to have an uncertainty of ± 80 K for this size collector.

Table 5. H_2 Raman Temperature Measurement Laser Energy Requirements for ± 30K

Spatial Resolution [cm]	F-Number [-]	Collector Diameter [cm]	Laser Energy Edge [J]	Center [J]
5	19	35	2.5	16
10	37	18	4.7	30
15	56	15	7.1	45

Possible interferences must be considered with any diagnostic measurements based on Raman scattering. The SSME flow is largely free of particles and has the low visible luminosity (Cikanek, et al., 1987) characteristic of hydrogen/oxygen combustion. At small Raman shifts the weak rotational Raman spectrum of water vapor (Murphy, 1977) overlaps the first few rotational Raman transitions of hydrogen. The vibrational Q-branch of oxygen lies near the S(5) line of hydrogen. It can interfere with low resolution measurements at the edge of the SSME exit flow, in the shear layer where atmospheric oxygen mixes with the nozzle flow, or in unburned regions if they exist.

Radiation from OH is fairly strong in the SSME exhaust, particularly in the shear flow where secondary combustion takes place and in the Mach disk.(Cikanek, et al ., 1987) Since this radiation is cw, it can be discriminated against by gated detection. More difficult is radiation from laser-excited OH fluorescence (Meijer, et al ., 1986). OH has bands from excited vibrational states in the $A \rightarrow X$ system (Dieke and Crosswhite, 1962) namely the 3-1 and 4-2 bands, which could interfere with the Q-branch of hydrogen. Previous studies have not reported emission from these transitions following photodissociation of water. The magnitude of emission from these states depends on the reaction path and vibrational-rotational product distribution. Oxygen LIF can also interfere to some extent with Raman spectra of hydrogen and water vapor. It is discussed in more detail later in this report.

Hargis (1981) recognized the potential signal enhancement with an excimer laser and demonstrated the detection of nitrogen at 10^{-4} Torr pressure. Excimer lasers operating with broadband output also have been previously used for combustion measurements. Kobayashi, et al. (1987) reported the wavelength scaling of Raman cross sections for a number of molecules of interest in combustion using ArF (193 nm), KrF (248 nm), XeCl (308 nm) and XeF (351 nm) excimer lasers. They demonstrated an enhancement of the cross section for oxygen, due to near resonance, for wavelengths less than 290 nm and concluded that the KrF laser represented the most suitable excimer source for flame Raman spectroscopy. They also measured temperature from Stokes to anti-Stokes ratios, and carbon dioxide concentration profiles in a premixed methane-air flame. Pitz, et al. (1990) used broadband KrF and XeF lasers for spontaneous Raman measurements in H_2/air flames. They observed laser induced fluorescence (LIF) interferences, which they were unable to identify due to lack of spectral resolution. More recently Pitz and his co-workers have used Raman scattering excited by a narrowband KrF laser to measure temperature and species concentrations in hydrogen-air diffusion flames (Cheng, et al., 1991a) and supersonic flames (Cheng, et al., 1991b).

Spontaneous Raman measurements in hydrogen-air combustion with a narrowband, tunable KrF laser were made. Narrowband operation is necessary to minimize interferences, which are unavoidable with broadband operation. These interferences arise from OH and O_2 laser induced fluorescence (Andresen, et al., 1988). The measurement apparatus used for Raman measurements and the hydrogen flames are described next. The results of measurements are then reported and the identification of the source of LIF interferences is discussed.

Raman Apparatus

A commercial KrF laser (Lambda-Physik EMG-160T-MSC) was used in the measurement system. In this laser, the tunable oscillator output is seeded into an unstable resonator amplifier. Raman scattered radiation is collected in a back-scattering configuration to utilize the predominantly horizontally polarized output of the laser as shown in Fig. 14. A cylindrical lens focuses the laser beam to an area approximately 100 microns by 8 mm. The focused beam dimensions were measured from burn patterns on exposed photographic paper. The horizontal focal area of the laser is rotated in a periscope to align with the vertical spectrometer slit. For detection, the 0.5 meter spectrometer is equipped with either a photomultiplier and gated integrator or a diode array. The sample volume viewed by the spectrograph is approximately 1 mm long, 15 microns high and 75 microns wide. Modification of the collection geometry would permit more efficient signal collection. The laser energy is 0.2 J per pulse. Diode array spectra shown later represent an accumulation of some 1000 to 2000 laser pulses.

The porous-plug burner is operated premixed with a mixture of hydrogen, air and nitrogen. Gas flow rates, measured with calibrated flowmeters, are adjusted to make the flame fuel-rich, with either 4 or 8 percent unburned hydrogen remaining in the post-flame gases. The excess nitrogen is added to the flow to maintain post-combustion gas at a temperature calculated (Gordon and McBride, 1971) at 1400 K, assuming adiabatic flow, so as to simulate conditions in the SSME exhaust. The gas temperature was measured with a 3 mil diameter Pt-Pt 10% Rh thermocouple coated with BeO-Yt_2O_3. The measured gas temperature after applying a correction for radiation is 1180 K. Spectra typically are measured 19 mm above the burner surface, i.e. in the post-flame region.

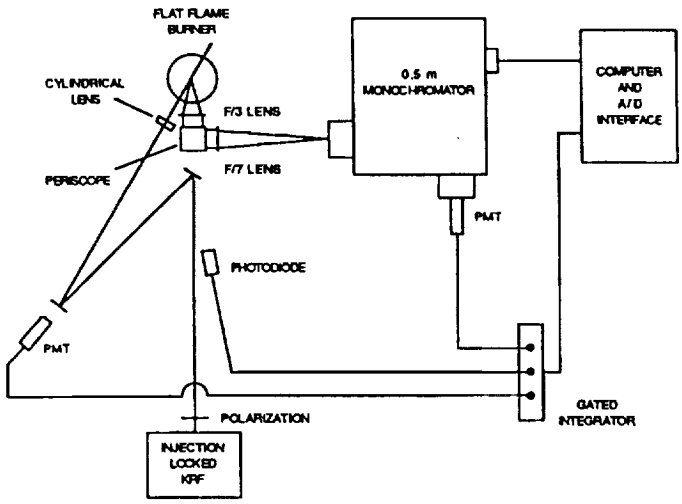

Figure 14. Schematic diagram of the excimer Raman experiments with a premixed flat flame burner.

Raman Measurements

Figure 15 shows a spectrum spanning a 10 nanometer wavelength range, including both H_2 and H_2O Raman Q-branches, with bandheads at 4155 and 3752 cm^{-1}, respectively. Individual components of the H_2 Q-branch near 277.2 nm are resolved and some structure is discernible in the H_2O spectrum with a bandhead at 273.4 nm.

A series of other peaks is also apparent at this particular laser frequency. These peaks are LIF from P, Q and R transitions of hydroxyl radical. Excitation of OH LIF following absorption of KrF laser radiation in the A^2 S-X^2 P_i (3,0) band was described by Andresen, et al. (1988), who found fifteen absorption lines within the nominal tuning range of 40,190 to 40,320 cm^{-1}. The emission lines, arising from transitions with in the (3,1) vibrational band, are labeled in Fig. 15. The transitions are connected to the $N = 11$ level of A^2 S ($v'=3$) which is populated by the (3,0)$Q_1(11)$ absorption at 248.352 nm. The laser is tuned to a position near the center of the tuning range. The wavelength of the laser has been determined by calibrating the spectra with a neon lamp in first order; Raman spectra are recorded in second order. The Raman shift and measured wavelength of Q(3) of H_2 are then used to calculate the laser wavelength; which, in this case, is determined to be 248.35 nm (vacuum). This agrees very well with the wavelength of the absorbing $Q_1(11)$ transition.

Figure 16 shows another laser tuning which excites a different triad of transitions corresponding to absorption by (3,0)$P_2(8)$ at 248.457 nm. The Raman spectra are the same, but shifted in wavelength. Determining the laser wavelength, as before, gives 248.47 nm, which is in satisfactory agreement with the known absorption wavelength.

Laser induced fluorescence interferences depend on the tuning of the laser with respect to absorbing species resonances. The dramatic effect of tuning is shown in Fig. 17, which presents a series

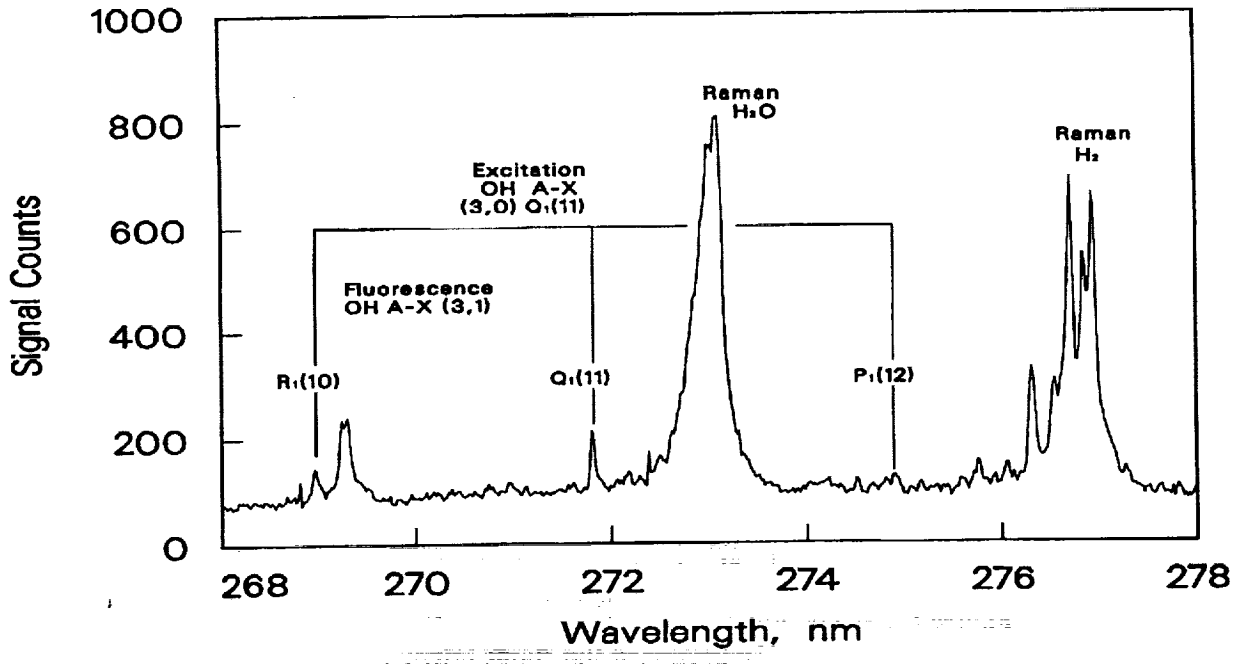

Figure 15. Spectrum of H_2 and H_2O in H_2–air N_2 flame. LIF from triplet of OH excited is identified. The laser wavelength is 248.35 nm.

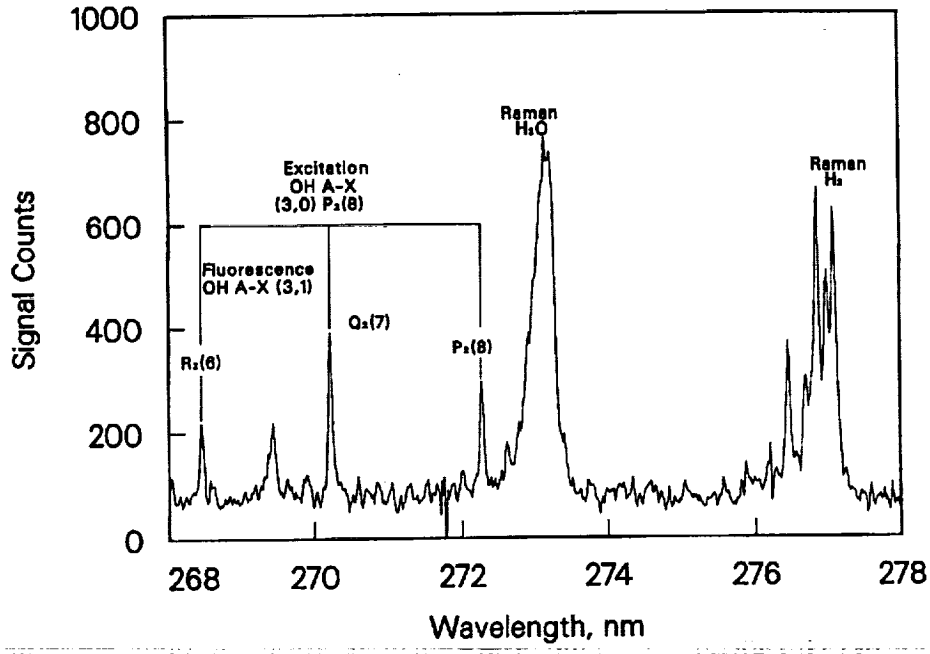

Figure 16. Spectrum of H_2 and H_2O Raman signatures and OH LIF with laser tuned to 248.47 nm.

of spectra at different laser frequencies separated by 1.68 cm^{-1}. These spectra were obtained in a small H_2 – air diffusion flame. First, note the Raman Q–branch of H_2O at 273.3 nm seen in all spectra.

Hydrogen would be at 277.1 nm were it not consumed at the measurement point in the flame. The strong triads of transitions in a and b are OH transitions. The absorbing transition in a is $P_2(8)$ which pumps the level radiating into $P_2(8)$, $Q_2(7)$ and $R_2(6)$. Spectrum b shows transitions excited by absorption on the satellite transition $P_{12}(8)$, which then radiates to $P_1(8)$, $Q_1(7)$ and $R_1(6)$. c and d show oxygen LIF P and R transitions (Andresen, et al., 1988) excited by absorption on 0,6 and 2,7 vibrational bands of the Schumann-Runge band. The oxygen fluorescence lies at 266.3-268.8 nm for $v',v'' = 0,8$ and 2,9 vibrational bands, and 276.3-278.4 nm for 0,9 and 2,10 bands. The latter bands interfere with H_2 Raman, when combustion is incomplete. Spectra e and f show water vapor Raman spectra that are relatively free of LIF interferences.

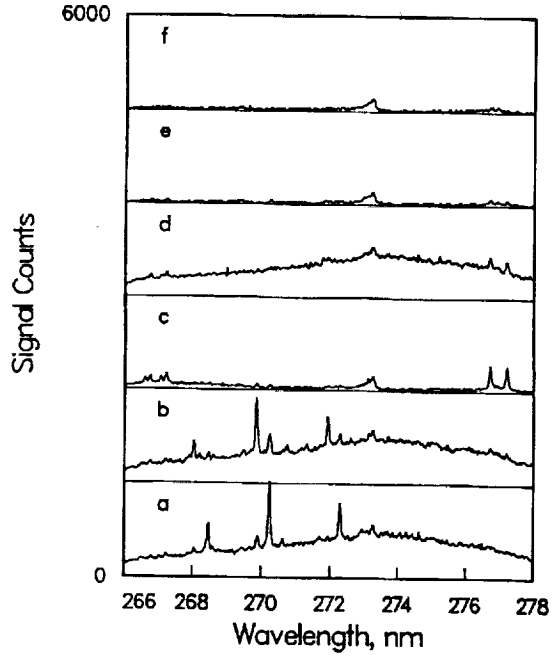

Figure 17. The effect of laser tuning on spectra in the H_2 and H_2O Raman Q-branch wavelength region. The laser is tuned in 1.68 cm^{-1} steps between the spectra.

The Raman Q-branch of hydrogen, measured in the premixed flame, is shown by the solid line Fig. 18. The dashed line is a calculation for 1200 K, appropriate to the thermocouple measured gas temperature. An instrument function for the spectrograph/OMA combination has been included in the calculation. The instrument function was determined independently by fitting the profiles of a number of well separated lines of a standard spectral lamp. The instrument function is dominated by the OMA detector (intensified diode array). The response profile consists of the combination of a sharp spike and a broad peak which is about 15 percent of the height of the spike and 4 times broader. Mathematically, the instrument function is fit with a double gaussian.

The accuracy of relative concentrations determined from uv Raman has been checked by comparison to the known reactant flowrates in the premixed flame. The species i population density, n_i, is related to the signal count, N_R, integrated across the Raman band:

$$N_R = \frac{E_L \sigma_i n_i l \Omega \varepsilon}{hck_i^S}$$

where E_L is the incident laser energy, s_i is the Raman cross section, l is the length of the scattering volume,W is the collection solid angle and e is the counting efficiency, which combines collection efficiency and detector efficiency. k^S_i is the Stokes-shifted energy of the photon scattered by species i and h and c are Planck's constant and the speed of light respectively. The relative H_2 and H_2O densities can be expressed as

$$\frac{n(H_2)}{n(H_2O)} = \frac{\sigma/k_s(H_2O)}{\sigma/k_s(H_2)} \frac{N_R(H_2)}{N_R(H_2O)}.$$

The ratio of the Raman cross sections is the most uncertain quantity in this expression. The range of literature values (Cherlow and Porto, 1976 and Inaba and Kobayasi, 1972 for the ratio $s(H_2)/s(H_2O)$ is 0.92 – 1.1, with stated accuracies of 10%. The uncertainty in the measured Raman counts is estimated to be about 7%.

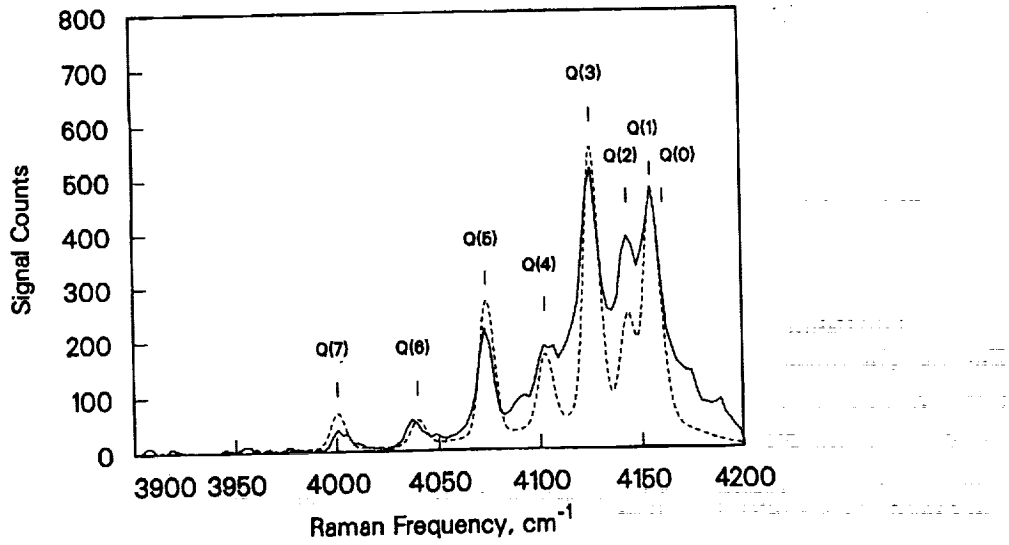

Figure 18. Raman spectrum of H_2 Q-branch in H_2-air-N_2 fuel-rich flame described in the text (solid line). The dashed line shows a spectrum calculated for a 1200 K temperature.

The measured ratio $N_R(H_2)/N_R(H_2O) = 0.76 \pm 0.05$ as determined from spectra shown in Figs. 15 and 16. Therefore the ratio of concentrations: $n(H_2)/n(H_2O) = 0.69 \pm 0.11$, measured in the post-flame gas. This ratio implies a fuel equivalence ratio, $f = 1.69 \pm 0.11$ which agrees within experimental error with the equivalence ratio determined by the gas flowmeters: f = 1.60.

Laser-Induced Fluorescence Interferences

The origin of the OH species observed in laser induced fluorescence is of interest. One source is flame chemistry, but KrF laser radiation is also known to produce OH by two-photon photodissociation of water vapor (Meijer, et al., 1986 and Fotakis et al., 1981). Ninety percent of the OH produced this way is in the ground electronic state. The remaining 10 percent is found in either $v' = 0$, or $v' = 1$ of the $A^2\Sigma$ state (Meijer, et al., 1986). If the OH arises from two-photon photodissociation, the laser-induced fluorescence nominally should scale as the square of the laser power. In the post-flame zone of the premixed flame, the measured OH LIF level relative to the (linear) Raman scattering remained constant when the power was reduced by one-half, supporting the flame chemistry as the origin of OH in these measurements.

The effect of laser energy on OH LIF has also been studied in the small H_2 diffusion flame. This flame is hotter, so higher OH levels are expected. Figure 19 shows the OH LIF signal for connected P, Q and R transitions measured as a function of laser energy. A small departure from linearity is present. A two level model was assumed in calculations to simulate the temporal behavior of OH levels pumped by uv radiation and to evaluate this measurement. The equations for the time dependence of the upper ($v'= 3$) and lower ($v''=0$) OH levels, N_2 and N_1 respectively are (Lucht, 1987):

$$\frac{dN_1}{dt} = - N_1 \frac{B_{12}}{c} I + N_2 \left(\frac{g_1}{g_2} \frac{B_{12}}{c} I + A_{21} + Q_{21} \right),$$

$$\frac{dN_2}{dt} = N_1 \frac{B_{12}}{c} I - N_2 \left(\frac{g_1}{g_2} \frac{B_{12}}{c} I + A_{21} + Q_{21} + P_2 \right),$$

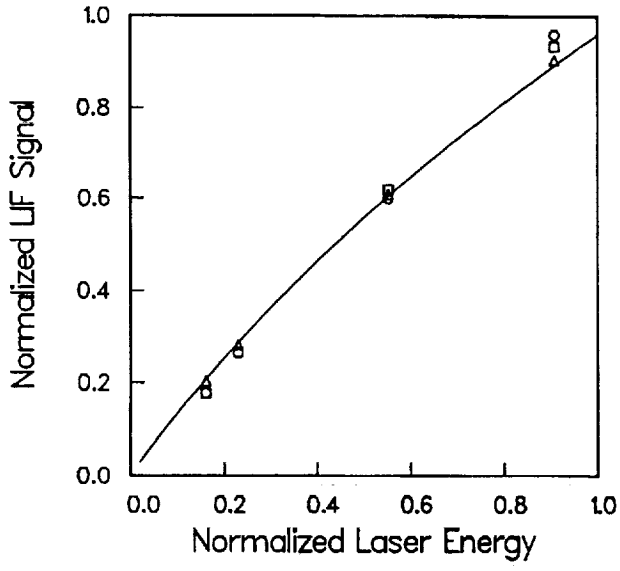

Figure 19. Dependence of OH LIF P, Q and R signals on KrF laser pulse energy. The solid line is the calculation described in the text.

where B_{ij} is the Einstein coefficient for stimulated emission, I is the laser spectral intensity, A is the Einstein coefficient for spontaneous emission, and Q and P are respectively the rates for quenching and predissociation. For these calculations $N_2 + N_1 \neq$ constant because of the predissociation term. Key data for the v'=3 level are not well known for OH. Andresen, et al., (1988) estimated a predissociation lifetime of 100 ps from the amount of rotational energy transfer evident in their OH LIF spectra. Sink, Bandrauk and Lefebvre (1980) have calculated predissociation linewidths for a number of vibrational levels. The radiative transition rates for many vibrational-rotational levels of OH have been calculated by Chidsey and Crosley (1980) but values for the levels of interest here are not included. The predissociation and quenching rates are the more important parameters. In the calculations herein: $I = 4.5 = 10^9$ W/cm at the maximum, $P = 10^{10}$ sec^{-1} and $B = 2.5 \times 10^{11}$ cm^2/J-sec. The model calculations, which include a gaussian temporal laser pulse indicate that predissociation dominates the loss mechanisms and determines the temporal evolution of the radiation driven populations. The LIF signal level, calculated as a function of laser spectral intensity, is shown by the solid line in Fig. 19. The calculations represent the data quite well, supporting the hypothesis of a flame chemistry source for the OH, as might be expected in this flame, and also indicate the onset of saturation.

All of the main OH branch transitions: 3-1, 3-2, and 3-3 bands, which fluoresce from the laser prepared A^2S state, do so at wavelengths that do not interfere seriously with either H_2 or H_2O Raman spectra with only one exception. Absorption at the A-X 3,0 $R_1(15)$ transition at 248.48 nm results in fluorescence from 3,1 $Q_1(16)$ at 275.54 nm (Dieke and Crosswhite, 1962) which is close to the Q(7) Raman transition of H_2. With excitation at the $R_1(15)$ wavelength, the H_2 Q(7) transition appears at 275.91 nm. However, the fractional population in N=15 is small for the relatively low temperature flames investigated here. For example, at 1200 K the population in the level absorbing $R_1(5)$ is more than an order of magnitude less than the population in the level absorbing $P_2(8)$. This makes the R_1 (15) difficult to observe, as was confirmed by the experiments. At 2000 K the population ratio n(N=15)/n(N=8) is about 0.2, so $R_1(15)$ becomes a more important potential interference in hotter flames. There are also several satellite branch transitions (Dieke and Crosswhite, 1962) radiating at wavelengths throughout the H_2 Q-branch, but the linestrengths of these are typically only 2 percent of the main transitions and at most 10 percent for low rotational levels. Therefore, for measurement near the flame front, where OH interferences are a concern, it is prudent perhaps to avoid the 3,0 $R_1(15)$ transition by suitably tuning the laser. On the other hand, measurements with a *broadband* KrF laser would excite all these transitions and entail degraded Raman signal-to-noise ratios because of the LIF interferences.

O_2 LIF can interfere with H_2 Raman in unburned flame zones, where O_2 and H_2 concentrations are high. For Raman measurements, the laser frequency should be chosen to avoid all these interferences, to the extent possible. Several windows exist in the excitation spectra of OH and O_2 in the KrF laser tuning range. A laser frequency near 40255 cm^{-1} avoids proximity to the OH and O_2 absorption and is close to the center of the KrF tuning range.

Conclusions for Raman Measurements

The LIF interference levels observed here do not preclude analysis of the Raman spectra for temperature or concentrations as demonstrated. Account would need to be made of the presence of

LIF for accurate measurements. OH concentrations could be deduced from spectra in cases where the predissociation rates are known and exceed quenching rates. In a broader range of combustion applications, the relative strength of OH interferences could vary widely, particularly in hotter flames. The source of OH has been shown, for these measurements, to be combustion chemistry, rather than two-photon photodissociation of water vapor. While it should be possible to tune the narrowband KrF laser to avoid these interferences, high injection locking efficiency will be an important requirement to achieve Raman spectra free of interferences.

VELOCITY MEASUREMENT WITH ENHANCED OH FLOW TAGGING

Velocity measurement by H_2O photolysis and laser-induced fluorescence of OH was conceived (Shirley and Boedeker, 1988 and Boedeker, 1989) as an attractive approach for high speed combustion-related environments, where high concentrations of water vapor would be present. An alternative tagging approach, vibrational excitation of O_2 and time delayed O_2 LIF, developed by Miles, *et al.*, (1989) does not apply to a fuel rich zone and may not have adequate tagged species lifetime for lean conditions. The H_2O photolysis-OH LIF concept was identified by Shirley and Boedeker (1988) in a study of potential approaches for measurement of temperature, species concentration and velocity in the exit plane of the space shuttle main engine (SSME). This velocity technique, also known as enhanced OH flow tagging, was demonstrated by Boedeker (1989) in a small supersonic free jet flow, containing water vapor, nitrogen and helium. This flow was formed by expansion from high pressure in a contoured nozzle to uniform conditions near Mach number M = 2, p = 1 atm, and T = 300 K. As such, the free jet contained a uniform supersonic core, with sharp shear layer gradient zones at the edges. The results of this demonstration clearly show the potential of the technique for accurate line imaging of velocity in high speed flows and detection of velocity gradient features. The studies in Boedeker (1989) and Boedeker (1992) also indicated the sensitivity of the photolysis technique at low water vapor concentrations and its possible application to general "moist" flows.

The potential of the enhanced OH concept for line imaging of non-uniform flows has been explored further by Goss, *et al.* (1991), using an underexpanded free jet. In addition they have determined that chemical lifetime of the OH photofragment can be long, about 150 microseconds, both for ambient flows and in a premixed propane-air flame. These studies help advance the H_2O photolysis-OH LIF concept to a level of performance close to the Miles (1989) work with O_2 tagging.

Depending on the application however, a number of issues remain to be addressed with the H_2O photolysis-OH LIF tagging approach. The kinetic model for lifetime of tagged OH suggests that in a fuel rich case the water forming reaction $OH + H_2 \rightarrow H_2O + H$ can be significant in reducing enhanced OH in a few microsecond period. This limitation on tagged OH lifetime needs to be investigated experimentally for the expected fuel rich SSME exit plane flow conditions. In addition, the SSME measurement system, Fig. 13, has to stand-off from the rocket exhaust for survivability, by an estimated distance of 7 meters. Intensities available in the laboratory for two-photon photolysis with a KrF excimer laser may not be attainable through the telescope which would focus the KrF laser beam into the rocket exhaust flow on the test stand. Moreover, SSME velocity measurements are desired simultaneously with temperature and species data acquired using uv Raman scattering from

the KrF laser beam. Photolysis of H_2O should not be so large that heating due to hot photofragments perturbs the local temperature level significantly. Further, an additional refinement arises because the KrF laser used for Raman measurements has to be line-narrowed and tunable, to resolve Raman spectral features and avoid spurious fluorescence interferences. The performance of the enhanced OH flow tagging velocity measurement needs to be confirmed in the presence of such narrowing and tuning.

For general application of enhanced OH flow tagging to moist flows, long delay times are desired, in order to make measurements at subsonic as well as supersonic velocities. The measurements of Goss, *et al.*, (1991) and Nejad (1991) indicate that long delay times are feasible. Kinetic model results obtained in the present studies indicate however, that a hydrogen peroxide, H_2O_2, mechanism may be involved in preserving the tagged species for such long times. Rapid recombination of OH to form H_2O_2 is predicted at 1 atm pressure and 300 K. Hydrogen peroxide photodissociates in a single photon absorption process to reform OH when exposed to radiation below about 400 nm. At 308 nm the process is dark, ground state OH being formed. If the uv excitation also happens to be tuned to excite OH electronically, then subsequent photons could be absorbed by OH during the laser pulse to yield OH fluorescence. Experiments are underway to check on this mechanism using a line-narrowed, high pulse energy 308 nm, XeCl excimer laser, tuned to excite OH 0-0 band fluorescence. Intensity variation measurements with this detection laser might reveal H_2O_2 through increased OH fluorescence due to photolysis at intensity levels beyond the expected saturation level.

In the enhanced OH flow tagging concept, a focused KrF (248 nm) excimer laser photodissociates H_2O by a two-photon process (Fotakis *et al.*, 1981, Meijer, *et al.*, 1986 and Engel *et al.*,1987), resulting in the creation of a small zone in which the hydroxyl radical concentration is enhanced above the background. A portion of the OH generated in the photofragmentation process is electronically excited and fluoresces. Both the laser pulse and fluorescence decay time are short, 10-30 nanoseconds. Hence, a fluorescence marker is created which can be used to locate the initial enhanced OH zone with an optical multichannel detector (OMD). The enhanced OH zone would be convected several millimeters in 1-2 microseconds at S SME exhaust velocities. The distance the enhanced OH zone moves would be measured with the OMD by inducing OH fluorescence with a time-delayed, uv pulsed dye laser, tuned to a single-photon electronic resonance as illustrated schematically in Fig. 20. This approach could be implemented with available lasers and detectors, is potentially a two dimensional method, and could be integrated easily with the uv Raman measurements in a diagnostic system. Self-absorption in background OH in the SSME exhaust flow may be present, but it should not affect the imaging of the key enhanced OH zones.

For single point data, the relative pulse shapes that should be seen by a multichannel detector with 1:1 imaging are shown in Fig. 21 for the case of a standard, commercially-available linear diode array. The initial and convected pulses are seen to be well resolved which should lead to higher accuracies than techniques using Doppler-shifted line profiles. At the expected laser focal diameters, each pulse spans a large number of channels. Some broadening of the convected pulse at the centerline will occur due to diffusion of initial enhanced OH, since kinetic effects likely are small. At the edge of the exit plane, diffusion of H atoms will play a role, since reaction kinetics likely are significant there in

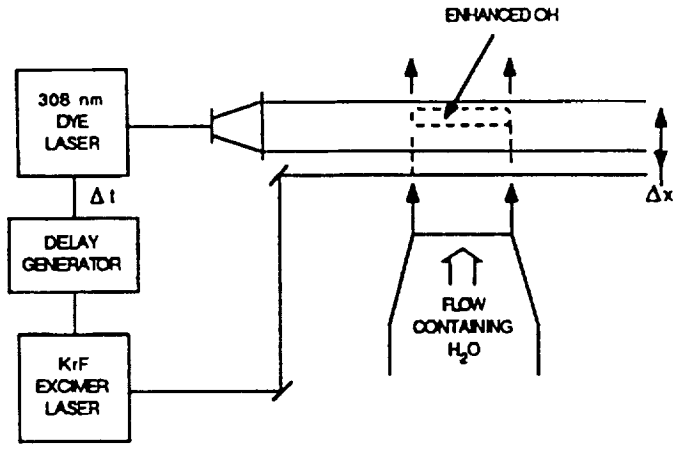

Figure 20. Flow tagging concept based on photodissociation of H_2O and tracking of OH.

sustaining OH concentration. However, the mean free path is small enough, probably about 0.01 mm at the centerline, that diffusion relative to convection should be about 10% or less throughout.

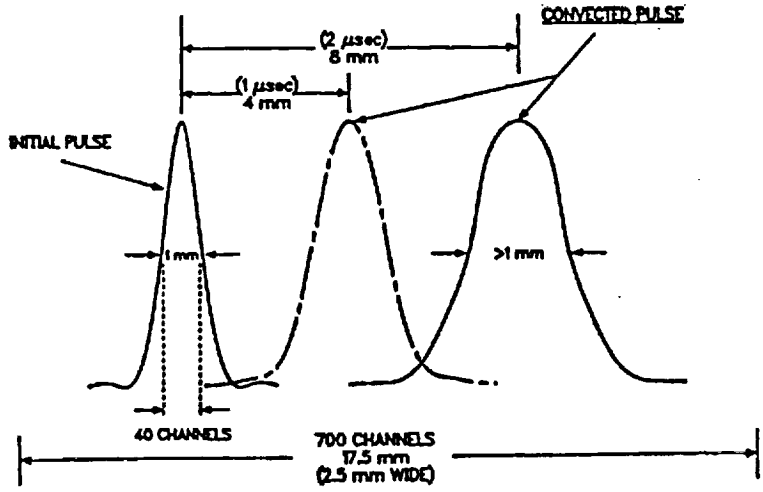

Figure 21. Representation of one-dimensional detection of enhanced OH signals with 1:1 imaging in a linear diode array.

Results in a N_2 Diluted Premixed H_2/Air Flame

The experimental configuration used for these studies is shown in Fig. 22. The KrF laser and the appropriate OH detection laser were aligned to pass over the center of a premixed porous bronze burner at a narrow crossing angle. The KrF laser was focused near the center of the burner and the detection laser beam conditioned to be somewhat larger than the KrF focal spot size. OH fluorescence was collected at an angle (20 – 90°) to the laser beams by a quartz lens and directed either to a photomultiplier (PMT) for temporal analysis, or to a 2-D optical multichannel analyzer (OMA) for spatial imaging of the enhanced OH fluorescence. The premixed flame was generally adjusted to be H_2 rich, about 24 mol% relative to the sum of H_2 and H_2O concentrations. In this manner results

would correspond to the expected concentration of H_2 in the SSME (H_2/O_2 rocket) exit plane flow (Shirley and Boedeker, 1988). In order to achieve low flame temperature, for simulation of temperature in the high Mach number SSME exhaust, additional N_2 diluent was used, beyond that present using air as the oxydizer. As a result, net H_2 concentration in these flames was about 5 mol%. Values of net H_2 concentration a factor of two lower and higher were used also. Adiabatic flame temperature was calculated to be about 1400 K. Heat balance of the burner cooling water and thermocouple measurements in the post flame gases indicate that, due to burner losses, actual temperature was about 1200 K.

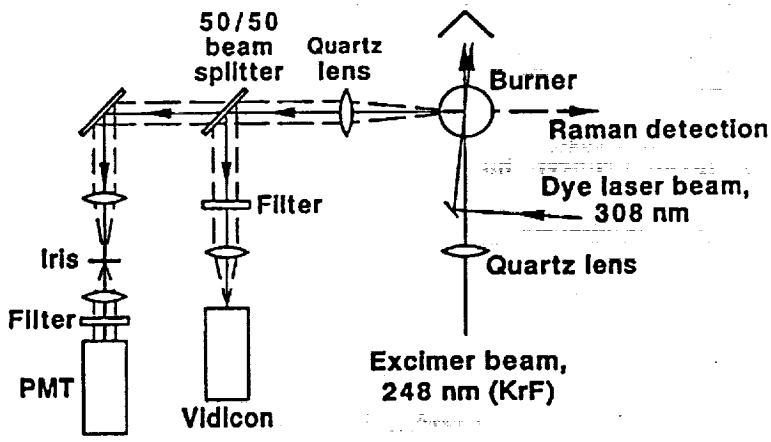

Figure 22. Optical detection system for enhanced flow-tagging measurements using two-photon photodissociation of H_2O.

Imaging Demonstration in Flame

Typical enhanced OH fluorescence imaging results obtained in the laboratory flame are shown in Fig. 23. A Nd:YAG pumped, frequency doubled dye laser was used for detection, tuned to excite OH 0-0 band fluorescence near 308 nm. A vidicon was used for spatial detection at about 1:1 magnification. Fluorescence was detected through a 310 nm, 1.5 nm FWHM, 6% transmission filter placed in the collimated portion of the vidicon signal path. The pulse energy of the KrF laser was about 200 mJ, tuned near the center of the gain profile. The KrF beam was focused over the burner to a spot size of 0.3-0.4 mm and positioned at a height of about 5 mm above the burner surface. The bottom trace in Fig. 23 shows that the excimer laser itself induced a small amount of OH fluorescence during the photolysis process (Meijer *et al.*,1986), which appears in a narrow spatial zone. The dye laser induced a stronger OH fluorescence (middle trace) by itself from flame generated OH, appearing in a broad 2-3 mm zone, representative of the size of this unfocused beam. The combined excimer-dye laser case (top trace) was obtained by timing the detection dye laser pulse to arrive 2 microseconds after the KrF laser. This combined effect trace shows that the KrF induced enhanced OH concentration is much larger than the flame background OH. The tagged zone created by the focused excimer appears as a sharp spike on top of a broad background signal. The 2 microsecond time delay between dye and excimer laser signals is useful for the SSME application where velocities exceed 4000 m/sec. The flow velocity in the flame is < 1 m/sec, too low to resolve in these studies, but the favorable enhanced OH lifetime results are evident. Further above the burner there is a reduced effect of

background OH, which is known to have a lower concentration higher in the post flame flow. Burner calibration studies are needed, but the background OH concentrations 5-10 mm above the surface of the burner in this flame are thought to be representative of background OH levels expected in the SSME exit plane.

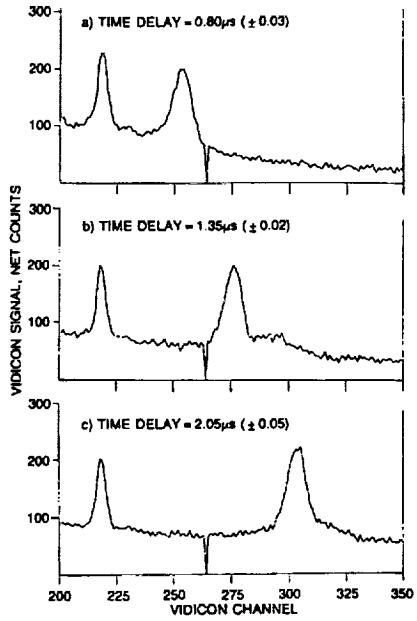

Figure 23. Vidicon spatial images of OH fluorescence in the M = 2 steam jet excited with the KrF excimer laser and the delayed dye laser at 308 nm.

Basic Photolytic and Flame Processes

The imaging demonstration results presented above were performed with typical laboratory parameters for the lasers, flame and detectors. As discussed earlier, further understanding of the roles played by KrF laser intensity and tuning, and fuel rich mixtures is needed in order to address the SSME rocket stand application. The relevant H_2O photolysis (Meijer *et al.*,1986) and flame kinetic processes are shown in Fig. 24. Two-photon photolysis of H_2O at 248 nm results in production of electronically excited and ground state OH, relative production depending on laser tuning. At high intensities a (2+1)REMPI process can compete with OH production and yield H_2O^+ ions. Water ion processes in the flame can be fast (Mul *et al.*, 1983) The hydronium ion, H_3O^+, forms quickly, producing an additional OH radical. At high photoionization levels subsequent dissociative recombination of hydronium ions (Meijer *et al.*,1986) can be significant, also producing an additional OH radical. These ionic OH formation steps apparently involve only ground state OH and are dark. At this time estimates of ion process significance for present conditions remain mostly qualitative.

The reactions involving OH and H_2O^+ in the fuel-rich hydrogen flame are:

$$H_2O^+ + H_2O \rightarrow H_3O^+ + OH$$
$$H_3O^+ + e^- \rightarrow H_2 + OH$$
$$OH + H_2 \leftrightarrow H_2O + H$$

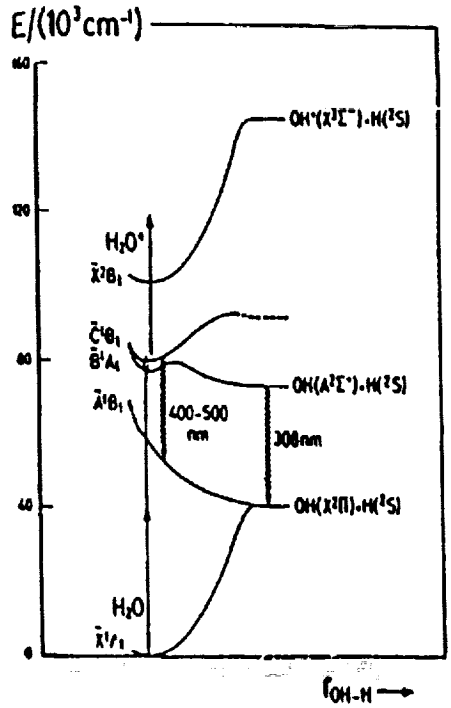

Figure 24. Two photon photolysis and ionization processes in water vapor. Diagram is taken from Meijer et al., (1986).

The final reaction is the water forming reaction discussed earlier. Calculations with the CHEMKIN code (Coltrin, et al., (1980), which does not consider the ionic reactions here, indicate that this water forming step is the key reaction in the fuel rich flame. Rapid production of equal enhanced levels of OH and H by photolysis tends to be followed by a reduction in OH and increase in H caused by a shifting of this reaction to the right to form a new partial equilibrium. Some predicted OH concentration decay results are shown in Fig. 25. These were obtained with CHEMKIN for assumed instantaneous 1000 PPM enhanced levels of OH and H and several values of H_2 concentration. The decay of OH is seen to be very sensitive to H_2 concentration. Near the level corresponding to the SSME case, H_2 = 0.044, OH concentration is predicted to be reduced by a factor of about 2 in 1 microsecond and a factor of 10 in 3 microseconds. Calculations at higher and lower values for initial OH and H concentrations show that relative decay predictions are reasonably similar to values shown in Fig. 25. Hence these calculations should provide a reasonable basis for comparison with experiment, even if quantitative results for enhanced OH produced from KrF photolysis are not known as yet.

Parametric Studies in Flame

OH Fluorescence Induced by KrF Excimer Laser

The effect of KrF excimer laser tuning and intensity on OH fluorescence induced directly during the 248 nm two-photon photolysis step was studied. This fluorescence could be used to mark the

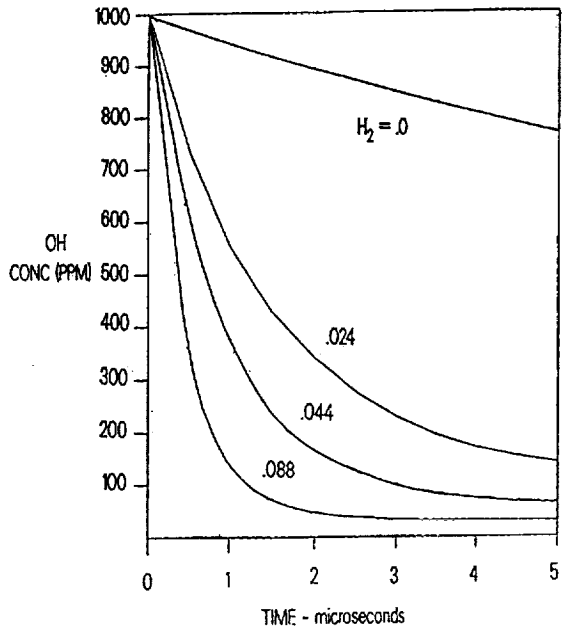

Figure 25. Predicted effect of hydrogen concentration on enhanced OH decay. H_2/O_2, CHEMKIN, 1200K, 1000 PPM OH, H H_2O Concentration 0.15, Balance N_2

initial location of the enhanced OH zone on the OMA. No detection laser was required to obtain this data, hence a wide bandwidth filter near 308 nm was employed with a PMT for OH fluorescence detection. A 2 meter focal length lens focused a well-locked, low divergence KrF beam to a spot size of about 0.3 mm. Low beam intensities were obtained, corresponding to levels investigated in basic studies (Meijer, et al., 1986), by using a beamsplitter to transmit only a small fraction of beam energy, and by including viewing of a larger spot, about 0.9 mm diameter, located 8 cm ahead of the focus. The KrF laser was tuned using a stepper motor to control the grating on the oscillator. Fluorescence was measured with a PMT whose output was monitored with an x-t recorder, synchronized with the stepper motor.

Results of the KrF induced fluorescence measurements are summarized in Table 6. Spectral structure normally associated with two-photon effects (Meijer, et al., 1986) at 248 nm in H_2O was not observed in the flame, at and ahead of the focus. Only a broadly shaped, noisy fluorescence signal profile was observed over the whole tuning range of the laser. However, some 2-photon related spectral structure was detected in moist room air for these intensities. High pressure and temperature, relative to the basic study results, are likely reasons for the masking of structure in the 1 atm flame. An exception was that a few narrow spectral features could be observed in the flame at the lowest intensity, 0.05 GW. These features are thought to represent single photon excitation of the predissociated OH 3-0 band near 248 nm (Meijer, et al., 1986), since the intensity of these lines increased as the KrF beam was located closer to the burner surface where OH concentrations were higher. As KrF laser intensity increased, saturation and two-photon intensity squared effects apparently reduced the relative strength of these sharp lines.

Table 6. Effect of KrF Excimer Laser Tuning on 248 nm Induced OH Fluorescence in Flame

Transmitted KrF Pulse Energy, 10 mJ
(95% net transmissive beamsplitters, 200 mJ pulse energy)
308 nm filter, FWHM = 25 nm

Viewpoint	Spot Size	Intensity	Source	Result
focus	0.3 mm	0.5 GW	Room H_2O	Some 2-photon-like Spectral Structure
focus	0.3 mm	0.5 GW	1200 K H_2/AIR/N_2 Flame	much less structure
8 cm ahead of focus	0.9 mm	0.5 GW	Room H_2O	Some 2-photon-like Spectral Structure
8 cm ahead of focus	0.9 mm	0.5 GW	1200 K H_2/AIR/N_2 Flame	a few narrow spectral features, otherwise little structure

Generation and Decay of Enhanced OH

For these measurements, which are temporal in nature, the PMT was used for detection of OH fluorescence. The detection laser in this case was the injection-locked 308 nm (XeCl) excimer laser, tuned to excite the $Q_1(3)$ 0-0 band transition of OH. In an eventual field diagnostic application, direct use of this tunable 308 nm excimer laser for OH detection would simplify the system and reduce cost. Detection was at a backscatter angle of about 20° to the laser beams. In order to reduce 308 nm Rayleigh scattering from the detection laser, the 310 nm narrowband filter, used in the imaging demonstration, was placed ahead of the PMT. The KrF laser was focused over the burner with a 2 m focal length lens. Focal spot size was measured to be about 0.3 mm, determined from 248 nm Rayleigh scattering imaging of the focal zone. Since this size is much smaller than expected in a rocket stand application, most measurements were made by placing the lens several centimeters closer to the burner, where the 248 nm spot size over the burner was more appropriate, about 1.1 mm average diameter, as measured from burnspots on photosensitive paper. The 100 mJ 308 nm excimer laser output beam was shaped and steered to achieve a small, low energy detection beam which overlapped the KrF beam over the burner. From measurements with various size apertures and a power meter, the 308 nm beam at the burner was uniform in intensity to about 1.5 mm diameter, and half intensity occurred at about 1.7 mm. Total 308 nm energy was about 1-1.2 mJ per pulse at the burner. Some saturation of OH fluorescence should have been present for this energy. Higher energies would have improved saturation but would also have increased Rayleigh scattering to unacceptable levels relative to fluorescence.

The timing of the two excimer lasers and a fast oscilloscope was controlled with a commercial multichannel digital delay generator. Photodiodes located behind final turning mirrors detected the arrival of KrF and XeCl laser beams at a position about 2 m ahead of the burner. The PMT and photodiode signal outputs were first detected with the fast oscilloscope to monitor timing of the KrF and XeCl excimer lasers and estimate the level of enhanced OH fluorescence relative to

flame-generated OH fluorescence. The photodiode signals then were used to trigger a gated integrator (BOXCAR) for quantitative recording of OH fluorescence signal levels from the PMT. Specifically, triggering of the BOXCAR with the XeCl laser photodiode pulse was used to acquire enhanced OH fluorescence decay data as the time delay between the XeCl detection laser and the KrF photolysis laser was increased. The BOXCAR signal output was read with an x-t chart recorder as the time delay was varied on the digital delay generator.

Enhanced OH decay data (Boedeker, 1992) obtained in the above manner are presented in Fig. 26, for full KrF beam energy, 200 mJ, and viewing of the large, 1.1 mm spot ahead of the focus. Measurements were made for three hydrogen concentrations, 0.02, 0.05, 0.09. The digital delay generator was set initially so the XeCl beam arrived 100 ns before the KrF beam. Hence, the initial part of each data trace records a fluorescence signal proportional to flame background OH concentration. At the arrow labeled "start" the digital delay was advanced 20 ns every 2 sec of elapsed time. Laser repetition rate, was 10 Hz and BOXCAR averaging set for 10 shots, hence signal response reached near steady state conditions during the 2 sec delay advance period. These data are shown replotted in Fig. 27, showing the nearly exponential decay at the three excess hydrogen flows.

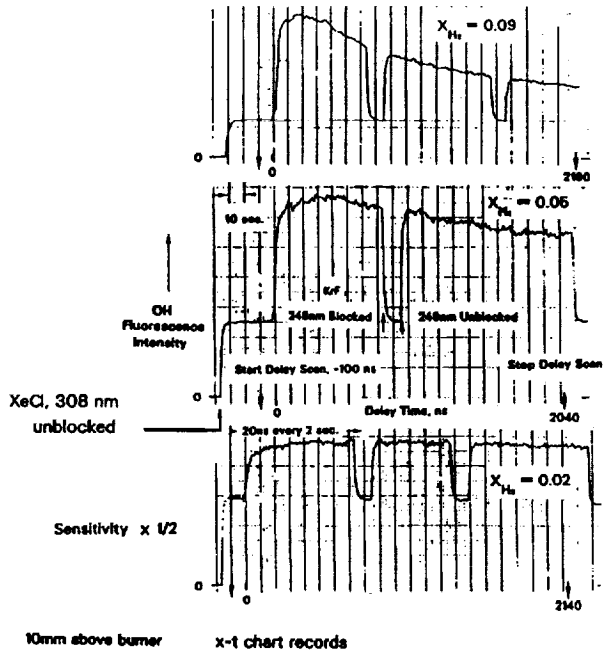

Figure 26. Effect of H_2 concentration on enhanced OH decay. The KrF pulse energy is 200 mJ and the LIF is measured 8 cm before the focal point. N_2 diluted, H_2-air flame, T = 1200K.

Intensity of the KrF laser was reduced a factor of two by reducing KrF pulse energy with a beamsplitter. Results presented in Boedeker (1992) indicated about a factor of two reduction in the enhanced OH signal relative to background OH. Finally the intensity of the KrF laser beam was increased significantly by moving the lens back to view the true focal zone. In this case, the KrF beam was much smaller than the 308 nm detection beam. The results shown replotted in Fig. 28, for 9 percent excess hydrogen, show a substantial increase in enhanced OH and a decrease in the decay rate of OH.

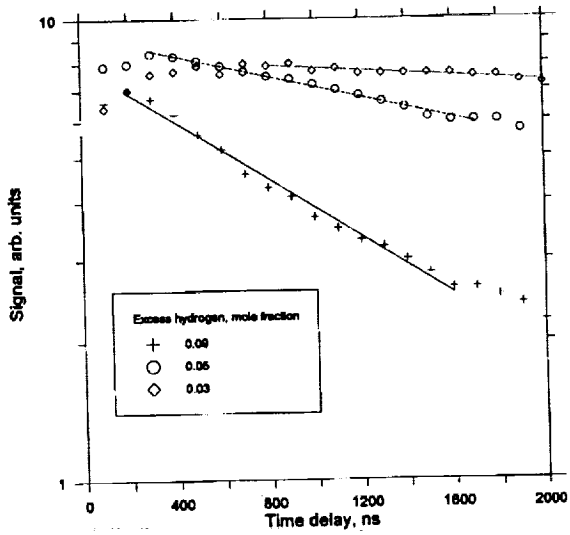

Figure 27. OH fluorescence decay curves as a function of excess hydrogen flow.

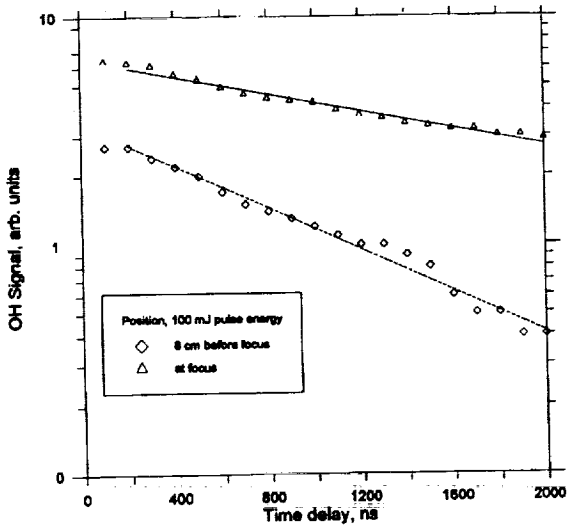

Figure 28. OH fluorescence decay curves showing the effect of laser intensity on the decay rate.

Discussion of Flame Results

Results in Figs. 26–28 show that background OH concentration decreased with increasing hydrogen concentration, as expected. The exact OH concentrations represented by these fluorescence levels are not known as yet. They could be obtained from uv absorption measurements with a dye laser beam or OH emission sources. These OH fluorescence levels correspond to OH concentrations attained after several milliseconds of kinetic decay from nonequilibrium flame front values near the burner surface. These flame front OH levels for the present 1200 K case are known to be much less than the typical 1% concentrations obtained in a diffusion flame, and the levels at the test location

above the burner will be even lower. Results are thought to be representative of the 100 PPM values expected in the SSME exit plane flow.

Enhancement of OH concentration due to water photolysis by KrF laser radiation is seen to be significant here relative to background OH, as indicated by the sharp rise in OH fluorescence as the detection laser was timed to arrive at and then after the KrF pulse. For the two weakest KrF intensities (Boedeker, 1992) OH fluorescence peaks about 200 – 400 ns after the KrF pulse. For the strongest intensity (Boedeker, 1992) OH fluorescence peaks at about a 100 ns delay. The OH is formed rotationally hot in the photolysis process. For these 1 atm flames several OH collisions should be occurring during the approximately 20 ns laser pulse. Hence rotational equilibration would be expected prior to these observed OH fluorescence maxima, and the results would suggest that OH concentration tended to increase by some process after the KrF pulse. One possibility would be dissociative recombination of hydronium ions, as discussed earlier.

Subsequent to the fluorescence maxima, OH fluorescence (and probably OH concentration) are seen in Fig. 25 to decay, at a rate that increases with increasing H_2 concentration. Qualitatively, this measured effect of increasing H_2 on OH decay agrees with the kinetic predictions, Fig. 25. Quantitatively, however, measured decay appears significantly slower than predicted by CHEMKIN. A factor of 2–20 decay in OH concentration is predicted by CHEMKIN at 2 microsecond delay for H_2 concentration variation from 0.02 to 0.09. Measurements here indicate a decay of only about 0 – 3 over this H_2 range. In general better agreement would be expected based on the known uncertainties in rates for the water forming reaction.

One key parameter in this comparison of model with experiment is the hydrogen concentration. A factor of two error in experimental settings for net H_2 concentration would be significant. In fact, the experimental results for H_2 = 0.02 look very much like results predicted for H_2 = 0. Experimental values should be accurate, based on 1% flow meter calibrations. However, because of the importance of the issue for rocket stand applications, a separate check on flowmeter settings has been performed through gas sampling and on-line mass spectrometric tests of O_2 relative to N_2. No O_2 was detected for the 0.02 H_2 case, and reduction in the H_2 flowmeter setting at constant air flow has yielded results for O_2 appearance in the mass spectrometer data that are consistent with the flowmeter calibrations. Hence the above data comparison with model appears valid. Diffusional effects here are not expected to be significant (H atom and OH), and would only serve to speed up the predicted decay of OH in the detection zone. One possibility is that ion reactions are more significant than initially anticipated, and should be investigated further.

Conclusions for Velocity Measurements in SSME Exit Plane

The results to date appear to be favorable for application of enhanced OH flow tagging to velocity measurements in the SSME exit plane, but specific factors need to be addressed in instrument design. For example, one important issue is the magnification required of the optic that images the enhanced OH at large stand-off distances onto the OMA. Working at 1 microsecond delay time the enhanced OH zone would be convected roughly 4 mm (4000 microns). Pixel size on detectors is typically 20–25 microns and for high accuracy, about 1%, the imaging optic should work near 1:1 magnification. This implies that this optic would probably be a large focal length off-axis toroidal

mirror. Such a mirror is expensive to manufacture. However, if delay times can be extended to 3-4 microseconds, then convection distance in the flow will increase to 12-16 mm, and reduction in image size by a factor of 3-4 may be tolerable without compromise of desired accuracy. On-axis mirror designs may then be practical. Present OH decay results suggest 3-4 microsecond delay times may be tolerable.

Such optical design issues suggest that further laboratory tests should be done to confirm the resolution of enhanced OH peak locations at parametric limits. Temperature at the edge of the SSME nozzle core flow increases to about 1400K. Additional imaging of the enhanced OH zones is desirable with available 2-D intensified arrays that are compatible with a rocket stand instrument package. The pressure at the SSME exit plane is less than 1 atm and diffusional effects expected at 3-4 microsecond delays should be considered further.

As discussed in the introduction, a diagnostic system is desired that would provide velocity data simultaneously with Raman species and temperature measurements in the SSME exit plane. Results presented here indicate that the velocity measurements can be accomplished with KrF intensities that are anticipated for a 7 meter stand-off distance. The laboratory results obtained with Rayleigh scattering imaging of an injection-locked KrF excimer laser indicate that excellent focussing can be attained with a plano-convex lens of 2 meter focal length. These results suggest that good telescope performance can be anticipated for a 7 meter stand-off design. The degree of commonality between components of the Raman and OH flow tagging systems will require further design and trade-off studies. The tuning required for Raman measurements does not appear to present any difficulty for velocity. Further work is required to confirm that the Raman system will provide required temperature precision at these attainable KrF intensities at the sub-atmospheric pressure SSME exit plane conditions.

REFERENCES

Andresen, P., Ondrey, G. S. and Titze, B. (1984), *Nuclear and Electron Dynamics in the Photodissociation of Water*, J. Chem. Phys., Vol. 80, p. 2548.

Andresen, P., A. Bath, W. Gröger, H. W. Lülf, G. Meijer and J. J. ter Meulen, (1988), *Laser-Induced Fluorescence with Tunable Excimer Lasers as a Possible Method for Instantaneous Temperature Field Measurements at High Pressures: Checks with an Atmospheric Flame*, Appl. Opt. Vol. 27, pp. 365-378.

Audeh, B. J. (1974), *Selected Boundary Layer Property Profiles at Several Axial Locations of the Boundary Layer of the Space Shuttle Orbiter Main Engine*, LMSC-HREC TN D390057, Contract NAS8-28609.

Becker, M., Robben, F. and Cattolica, R. (1973), *Velocity Distribution in Hypersonic Helium Flow Near the Leading Edge of a Flat Plate*, AIAA Paper No. 73-691.

Boedeker, L. R. (1959), *A Sharp Focusing Schlieren System for Wind Tunnel Application*, Masters Thesis, MIT Dept. of Aeronautics and Astronautics.

Boedeker, L. R. (1989), *Velocity Measurement by H_2O Photolysis and Laser-Induced Fluorescence of OH*, Opt. Letts., Vol. 14, p. 473-475.

Boedeker, L. R. (1992), *Velocity Measurements in Rocket and General Aerodynamic Flow by Photolysis of H_2O and Laser Induced Fluorescence of OH*, AIAA Paper 92-0003.

Bohn, W. L., Beth, M. U. and Nedder, G. (1985), *On Spectroscopic Measurements of Velocity Profiles and Non-Equilibrium Radial Temperatures in an Argon Plasma Jet*, J. Quant. Spectrosc. Radiat. Trans., Vol. 7, pp. 661-676.

Cattolica, R., Robben, F. and Talbot, L. (1976), *The Interpretation of the Spectral Structure of Rayleigh Scattered Light from Combustion Gases*, AIAA Paper No. 76-31.

Chandra, S., Compaan, A. and Wiener-Avnear, E. (1978), *Coherent Raman Scattering with Three Lasers*, Appl. Phys. Lett., Vol. 33, pp. 867-869.

Cheng, T. S., J. A. Wehrmeyer and R. W. Pitz, (1991a), *Simultaneous Temperature and Multi-Species Measurement in a Lifted Flame by a KrF Excimer Laser*, AIAA Paper 91-0181.

Cheng, T. S., J. A. Wehrmeyer, R. W. Pitz, O. Jarrett, Jr. and G. B. Northam (1991b), *Finite-Rate Chemistry Effects in a Mach 2 Reacting Flow*, AIAA Paper 91-2320.

Cherlow, J. M. and S. P. S. Porto (1976), *Laser Spectroscopy of Gases* in Laser Spectroscopy of Atoms and Molecules, H. Walther, Ed. (Springer-Verlag, Berlin).

Chidsey, I. L. and D. R. Crosley (1980), *Calculated Rotational Transition Probabilities for the A-X System of OH*, J. Quant. Spectrosc. Radiat. Trans., Vol. 23, pp. 187-199 and reference 13 therein.

Chou, M.S. and Dean, A. M. (1985), *Excimer Laser Perturbations of Methane Flames: High Temperature Reactions of OH and CH*, Intl. J. Chem. Kinetics, Vol. 17, pp. 1103-1118.

Cikanek, H. A., W. T. Powers, R. Eskridge, W. J. Phillips, F. G. Sherrell, W. K. McGregor and V. A. Zaccardi, (1987), *Space Shuttle Main Engine Plume Spectral Monitoring Preliminary Results*, AIAA Paper 87-1792.

Coltrin, M. E., R. J. Kee and F. M. Rupley (1980), Sandia National Laboratories Report, SAND90-8003.

Compaan, A. and Chandra, S. (1979). *Coherent Anti-Stokes Raman Scattering With Counterpropagating Laser Beams*, Opt. Lett., Vol. 4, pp. 170-172.

Dieke, G. H. and H. M. Crosswhite, (1962), *The Ultraviolet Bands of OH, Fundamental Data*, J. Quant. Spectrosc. Radiat. Trans., Vol. 2, p. 97-199.

Eckbreth, A. C. and Anderson, T. J. (1985), *Dual Broadband CARS for Simultaneous, Multiple Species Measurements*, Appl. Opt., Vol. 24, pp. 2731-2736.

Engel, V., G. Meijer, A. Bath, P. Andresen and R. Schenke (1987), *The C-A Emission in Water: Theory and Experiment*, J. Chem. Phys. Vol. 87, pp. 4310-4314.

Exton, R. J. and M. E. Hillard (1986), *Raman Doppler Velocimetry: A Unified Approach for Measuring Molecular Flow Velocity, Temperature, and Pressure*, Appl. Opt., Vol. 25, p. 14.

Fabelinski, I. L. (1968). Molecular Scattering of Light, Plenum Press, New York, p. 6.

Fotakis, C., McKendrick, C. B. and Donovan, R. J. (1981), *Two-Photon Excitation of H_2O and D_2O With a KrF Laser (248 nm): Photofragment Fluorescence From OH and OD($A^2\Sigma^+$)*, Chem. Phys. Lett., Vol. 80, p. 598.

Gaydon, A. G. (1974). The Spectroscopy of Flames (John Wiley and Sons, New York).

Gordon, S. and B. J. McBride (1971), NASA Report SP-73.

Gross, K., (NASA-Marshall) Private communication.

Gustafson, E.K., McDaniel, J. C. and Byer, R. L. (1981), *CARS Measurement of Velocity in a Supersonic Jet*, IEEE J. Quant. Electr., Vol. QE-17, pp. 2258-2259.

Hall, R. J. and Eckbreth, A. C. (1984), *Coherent Anti-Stokes Raman Spectroscopy (CARS): Application to Combustion Diagnostics, in Laser Applications*, Vol. 5, Academic Press, New York, p. 213.

Hargis, Jr., P. J. (1981), *Trace Detection of N_2 by KrF-Laser-Excited Spontaneous Raman Spectroscopy*, Appl. Opt., Vol. 20, 149-152.

Hiller, B. and Hanson, R. K. (1985), *Two-Frequency Laser-Induced Fluorescence Technique for Rapid Velocity-field Measurements in Gas Flows*, Opt. Lett., Vol. 10, p. 206.

Hodgson, A., Simons, J. P., Ashfold, M. N. R., Bayley, J. M. and Dixon, R. N. (1984), *Quantum-State-Selected Photodissociation of $H_2O(C^1B_1)$*, Chem. Phys. Lett., Vol. 107, pp. 1-5.

Inaba, H. and T. Kobayasi (1972), *Laser-Raman Radar-Laser-Raman Scattering Methods for Remote Detection and Analysis of Atmospheric Pollution*, Opto-Elect. Vol. 4, p. 101.

Kobayashi, T., M. Konishi, M. Ohtaka, S. Taki, M. Ueda, K. Kagawa and H. Inaba (1987), *Application of UV and VUV Excimer Lasers in Combustion Measurements Using Enhanced Raman Scattering*, Paper 5.4 in *Laser Diagnostics and Modeling Combustion*, K. Iinuma, T. Asanuma, T. Ohsawa and S. Taki, ed., (Springer-Verlag, Berlin), p 133.

Landau L. D. and Lifshitz, E. M. (1960), Electrodynamics of Continuous Media, (Plenum Press, New York), Chapt. XIV, p. 387.

Lucht, R. P., Sweeney, D. W. and Laurendeau, N. M. (1983), *Laser-Saturated Fluorescence Measurements of OH Concentration in Flames*, Combust. Flame, Vol. 50, pp. 189-205.

Lucht, R. P. (1987), *Applications of Laser-Induced Fluorescence Spectroscopy for Combustion and Plasma Diagnostics*, in Laser Spectroscopy and Its Applications, L. J.Radziemski, R.W. Solarz and J. M.Paisner, eds. (Marcel Dekker, New York).

McDaniel, J. C., Hiller, B. and Hanson, R. K. (1983), *Simultaneous Multiplepoint Velocity Measurements Using Laser-Induced Iodine Fluorescence*, Opt. Lett., Vol. 8, p. 51.

Meijer, G., terMeulen, J. J., Andresen, P. and Bath, A. (1986), *Sensitive Quantum State Selective Detection of H_2O and D_2O by (2+1) Resonance Enhanced Multiphoton Ionization*, J. Chem. Phys., Vol. 85, p. 6914-6922.

Miles, R., Cohen, C., Connors, J., Howard, P., Huang, S., Markovitz, E. and Russell, G. (1987), *Velocity Measurements by Vibrational Tagging and Fluorescent Probing of Oxygen*, Opt. Letts. Vol. 12, p. 861.

Murphy, W. F. (1977), *The Rayleigh Depolarization Ratio and Rotational Raman Spectrum of Water Vapor and the Polarizability Components for the Water Molecule*, J. Chem. Phys., Vol. 67, pp. 5877-5882.

Nejad, A. S. (1991), *Flow-Tagging Velocimetry using UV-Photodissociation of Water Vapor*, AFOSR Contractor's Meeting in Propulsion, U. Colorado, Boulder CO.

Pitz, R. W., J. A. Wehrmeyer, J. M. Bowling and T. S. Cheng (1990), *Single Pulse Vibrational Raman Scattering by a Broadband KrF Excimer Laser in a Hydrogen-Air Flame,* Appl. Opt., Vol. 29, p. 2325.

Papagiannakopoulos, P. and C. Fotakis (1985), *Kinetic Studies of $OH(A^2\Sigma^+)$Generated by Two-Photon Excitation of H_2O at 248 nm',* J. Phys. Chem. Vol. 89, pp. 3439-3441.

Rahn, L. A. and Greenhalgh, D. A. (1986), *High-Resolution Inverse Raman Spectroscopy of the ν_1 Band of Water Vapor*, J. Molec. Spectr., Vol. 119, pp. 11-21.

Rose, A. and Gupta, R. (1985), *Application of Photothermal Deflection Technique to Flow-Velocity Measurements in a Flame*, Opt. Lett.,Vol. 10, p. 532.

Shirley, J. A. (1986), *Fiber Optic Raman Thermometer for Space Shuttle Main Engine Preburner Profiling*, Presented at 1986 Conference on Advanced Earth-to-Orbit Propulsion Technology, George C. Marshall Space Flight Center, Huntsville, AL, May 13-15, 1986.

Shirley, J. A. (1992), *Fiber Optic Raman Thermometer for Profiling the Space Shuttle Main Engine'*, Final Report R92-957262-F, NASA Contract NAS8-34655.

Shirley, J. A. and L. R. Boedeker (1988), *Non-Intrusive Space Shuttle Main Engine Exit Diagnostics*, AIAA Paper 88-3038.

Sink, M. L., A. D. Bandrauk, and R. Lefebvre (1980), *Theoretical Analysis of the predissociation of the $A^2\Sigma^+$ state of OH*, J. Chem. Phys. Vol. 73, p. 4451-4459.

Smith, S. D. (1980), *Sea Level Space Shuttle Main Engine Exhaust Plume Definition*, Lockheed Huntsville Research & Engineering Center Technical Note LMSC-HREC TN D698355, Contract NAS8-33719.

Watanabe, K. and Zelikoff, M. (1953), *Absorption Coefficients of Water Vapor in the Vacuum Ultraviolet*, J. Opt. Soc. Am. Vol. 43, p. 753.

Yip, S. (1970), *Rayleigh Scattering in Dilute Gases*, J. Acoust. Soc. of Am., Vol. 49, pp. 941-949.